

UCSF

UC San Francisco Previously Published Works

Title

Bespoke library docking for 5-HT_{2A} receptor agonists with antidepressant activity

Permalink

<https://escholarship.org/uc/item/87f9q9sd>

Journal

Nature, 610(7932)

ISSN

0028-0836

Authors

Kaplan, Anat Levit

Confair, Danielle N

Kim, Kuglae

et al.

Publication Date

2022-10-20

DOI

10.1038/s41586-022-05258-z

Peer reviewed



Published in final edited form as:

Nature. 2022 October ; 610(7932): 582–591. doi:10.1038/s41586-022-05258-z.

Bespoke library docking for 5-HT_{2A} receptor agonists with anti-depressant activity

Anat Levit Kaplan^{†,1}, Danielle N. Confair^{†,2}, Kuglae Kim^{†,3,13}, Ximena Barros-Álvarez^{†,4}, Ramona M. Rodriguez^{5,6}, Ying Yang¹, Oh Sang Kweon², Tao Che⁷, John McCorvy⁸, David N. Kamber², James P. Phelan², Luan Carvalho Martins^{1,9}, Vladimir M. Pogorelov⁵, Jeffrey F. DiBerto³, Samuel T. Slocum³, Xi-Ping Huang¹⁰, Jain Manish Kumar³, Michael J. Robertson⁴, Ouliana Panova⁴, Alpay B. Seven⁴, Autumn Q. Wetsel⁵, William C. Wetsel^{*,5,6,11}, John J. Irwin^{*,1}, Georgios Skiniotis^{*,4}, Brian K. Shoichet^{*,1}, Bryan L. Roth^{*,3,12}, Jonathan A. Ellman^{*,2}

¹Department of Pharmaceutical Chemistry, University of California, San Francisco, CA, USA

²Department of Chemistry, Yale University, New Haven, CT, USA

³Department of Pharmacology, University of North Carolina, Chapel Hill School of Medicine, Chapel Hill, NC, USA

⁴Department of Molecular and Cellular Physiology, Stanford University School of Medicine, Stanford, CA, USA

⁵Department of Psychiatry and Behavioral Sciences, Duke University Medical Center, Durham, NC, USA

⁶Mouse Behavioral and Neuroendocrine Analysis Core Facility, Duke University Medical Center, Durham, NC, USA

⁷Center for Clinical Pharmacology, Department of Anesthesiology, Washington University School of Medicine, Saint Louis, MO, USA

*Corresponding authors. william.wetsel@duke.edu, jir332@gmail.com, yiorgo@stanford.edu, bshoichet@gmail.com, bryan_roth@med.unc.edu, jonathan.ellman@yale.edu.

[†]These authors contributed equally.

Author Contributions: The study was conceived by JAE, JJI, & BKS, and was designed by JAE, BLR, BKS, GS, JJI, ALK, DNC, KK, & X B-Á. ALK conducted the docking calculations and the cheminformatics, YY & LCM conducted MD and FEP+ calculations, JJI designed and implemented the virtual library and conducted the cheminformatics. DNC, DNK, & OSK synthesized and purified all compounds. JPP performed functional group compatibility screens. KK conducted the molecular pharmacology, assisted by TC, JM, STS, JMK, & JFD. X-PH conducted and supervised off-target activity assays. KK produced and purified the 5-HT_{2A}R, while X B-Á determined the structure of the agonist-complex, assisted by MJR, OP, & ABS. RMR, VMP, & WCW conducted the behavioral studies and were assisted by AQW. These studies were designed by WCW & BLR, some of the behavioral methods were written by AQW and the remainder were written by WCW with data analysis by RMR and graphing by WCW, VMP, & RMR. JAE, BLR, BKS, GS, JJI, ALK, DNC, KK, & X B-Á drafted the original manuscript; all authors reviewed the manuscript prior to submission.

Competing Interests: No other authors declare a competing interest.

Additional Information: Supplementary Information is available for this paper. Request for reprints should be addressed to Jonathan A. Ellman (jonathan.ellman@yale.edu), Bryan L. Roth (bryan_roth@med.unc.edu) and Brian K. Shoichet (bshoichet@gmail.com). Requests for chemical compounds should be addressed to Jonathan A. Ellman (jonathan.ellman@yale.edu) and Bryan Roth (bryan_roth@med.unc.edu). Requests for *in vitro* pharmacology reagents should be addressed to Bryan L. Roth (bryan_roth@med.unc.edu). Requests for computational data and results should be addressed to Brian K. Shoichet (bshoichet@gmail.com) or John J. Irwin (jir332@gmail.com). Questions regarding behavioral pharmacology should be addressed to William C. Wetsel (william.wetsel@duke.edu), and questions on structure determination should be addressed to Georgios Skiniotis (yiorgo@stanford.edu). Reprints and permissions information is available at www.nature.com/reprints.

- ⁸Medical College of Wisconsin, Department of Cell Biology, Neurobiology and Anatomy, Milwaukee, WI, USA
- ⁹Biochemistry Department, Institute for Biological Sciences, Federal University of Minas Gerais, Belo Horizonte, Brazil
- ¹⁰National Institute of Mental Health Psychoactive Drug Screening Program, University of North Carolina Chapel Hill School of Medicine, Chapel Hill, NC, USA
- ¹¹Departments of Cell Biology and Neurobiology, Duke University Medical Center, Durham, NC, USA
- ¹²Division of Chemical Biology and Medicinal Chemistry, Eshelman School of Pharmacy, University of North Carolina Chapel Hill, NC, USA
- ¹³Department of Pharmacy, Yonsei University, Incheon, Republic of Korea

Summary

There is much interest in screening ultra-large chemical libraries for ligand discovery, both empirically and computationally¹⁻⁴. Efforts have focused on readily synthesizable molecules, inevitably leaving many chemotypes unexplored. Here we investigate structure-based docking of a bespoke virtual library of tetrahydropyridines, a scaffold poorly sampled by a general billion-molecule virtual library but well-suited to many aminergic G protein-coupled receptors. Using three inputs, each with diverse available derivatives, a one pot C–H alkenylation, electrocyclization, and reduction provides the tetrahydropyridine core with up to six sites of derivatization⁵⁻⁷. Docking a virtual library of 75 million tetrahydropyridines against a model of the serotonin 5-HT_{2A} receptor (5-HT_{2A}R) led to synthesis and testing of 17 initial molecules. Four had low μM activities against either the 5-HT_{2A} or 5-HT_{2B} receptors. Structure-based optimization led to 5-HT_{2A}R agonists (**R**)-**69** and (**R**)-**70** with EC₅₀s of 41 and 110 nM and unusual signaling kinetics differing from psychedelic 5-HT_{2A}R agonists. Cryo-EM structural analysis confirmed the predicted binding mode to the 5-HT_{2A}R. The favorable physical properties of these new agonists conferred high brain permeability, enabling mouse behavioral assays. Intriguingly, neither had psychedelic activity, in contrast to classic 5-HT_{2A}R agonists, while both had potent anti-depressant activity in mouse models and were equi-efficacious to anti-depressants like fluoxetine at as little as 1/40th the dose. Prospects for using bespoke virtual libraries to sample pharmacologically-relevant chemical space will be considered.

Introduction

The advent of DNA-encoded and virtual libraries has led to a renaissance in ultra-large sets of molecules in early ligand discovery.¹ In particular, the virtual libraries now exceed 20 billion enumerated, readily accessible molecules. In docking screens, these virtual libraries have explored new chemotypes well-suited to receptor sites, discovering ligands with potencies in the mid-pM to low-nM range²⁻⁴. This represents a substantial improvement from screens of smaller, “in-stock” libraries of several million molecules against the same targets. The virtual libraries enumerate diverse chemotypes, reflecting the synthetic products of >120,000 building-blocks synthesized via >140 two-component reactions. Nevertheless,

the vastness of chemical space ensures that many interesting chemotypes are inevitably absent or under-sampled by both virtual and DNA-encoded libraries.

The six-membered nitrogen heterocycles piperidine and pyridine are two of the top three most frequent ring systems among FDA approved drugs (Extended Data Table 1). In particular, the non-aromatic piperidine scaffold has several desirable features, such as a basic nitrogen that contributes to aqueous solubility and hydrogen-bonding interactions, high sp^3 bond content with a three-dimensional rather than planar display⁸, and multiple sites for introducing substituents including at stereogenic centers. Tetrahydropyridines (THP) are a much less investigated class of six-membered nitrogen heterocycles that are intermediate in unsaturation between pyridines and piperidines with the same favorable attributes as piperidines. While THPs are present in several natural product-derived drugs that include the psychedelic lysergic acid diethylamide (LSD), the antimigraine drug ergotamine, anticancer agents like vinblastine and vincristine, and the antiprotozoal agent dehydroemetine (Figure 1a)⁹, the scaffold is under-represented in most libraries compared to its congeners piperidine and pyridine (Extended Data Table 1). In particular, while piperidine and pyridine occur in a startling 16 to 18% of the molecules in the unbiased REAL make-on-demand library, THPs comprised only 0.35% (Extended Data Table 1).

Obtaining a diverse display of functionality at different sites about the 6-membered ring in piperidines and THPs is synthetically challenging. Recently, we have described new, convergent routes to access three THP subtypes [(±)-**1** to (±)-**3**] with six sites of derivatization from commercially-available starting materials (Figure 1b)⁵⁻⁷. The large space defined by such derivatives, their functionally congested, geometrically complex structures, and their under-representation in general libraries (Extended Data Table 1)¹⁰, makes them interesting to explore as central scaffolds for large virtual libraries well-suited to structure-based molecular docking.

Accordingly, we calculated a library of over 75 million virtual tetrahydropyridines, built around commercially available building blocks and restricted to products with “lead-like” physical properties (e.g., 350 amu, $cLogP > 3.5$)^{11,12}. The cationic nature of these molecules at physiological pH makes them suitable as ligands for aminergic GPCRs, including the 5-HT_{2A} serotonin receptor (5-HT_{2A}R). The 5-HT_{2A}R is a target of much interest, owing to its role in treating psychiatric disorders including schizophrenia, depression, and anxiety¹³⁻¹⁵. The 5-HT_{2A}R also represents the canonical molecular target for LSD-like psychedelic drugs¹⁶, which have recently gained prominence as potential therapeutics for depression and anxiety¹⁷. With hallucination remaining a liability, a goal in this area is the development of drug-leads that retain anti-depressant and anxiolytic properties without psychedelic activity. Progress towards such leads and chemical probes against the 5-HT_{2A}R has been slowed by the need for selectivity over related off-targets, such as 5-HT_{2B}R, versus other receptors such as the serotonin transporter (SERT), and for functional selectivity in signaling (i.e., for G protein vs. β -arrestin recruitment^{16,18-21}). Collectively, these features make the 5-HT_{2A}R a therapeutically worthy yet challenging target. Meanwhile, the receptor’s small and well-formed orthosteric site¹⁶ makes it a favorable target for docking this particular virtual library.

We therefore explored docking to prioritize selective 5-HT_{2A}R ligands from among the 75 million molecule virtual library. Here we consider the mechanics of calculating a large library around a specific scaffold and reaction and synthesizing docking-prioritized molecules from such a large space, and whether this approach to discover and optimize potent and selective ligands is useful. Implications for the creation and exploration of bespoke libraries around interesting scaffolds more generally will also be considered.

Results

Virtual library calculation.

Tetrahydropyridine subtypes (±)-**1** and (±)-**2** were prepared from three readily available inputs: primary amines **4**, α,β-unsaturated carbonyl compounds **5**, and internal alkynes **6** (Figure 1b). Tetrahydropyridine subtype (±)-**3** was prepared from primary amines **4**, α,β-unsaturated carbonyl compounds **5**, and trimethylsilyl (TMS) alkynes **7**. A broad range of functional groups, including many different types of nitrogen heterocycles, were found to be compatible with the reaction sequence as determined by a functional group screen (Supplementary Figure 1). Heterocycle N–H functionality was incompatible with the chemistry, but this could be overcome by straightforward *N*-protection. Consequently, these inputs and restraints were also included in the virtual library. To simplify library synthesis and analysis, only achiral, single isomer inputs were included. Inputs with undesirable functionality like nitro groups, or molecules with too many rotatable bonds, were discarded. To generate library members with druglike physical properties, a molecular weight cutoff of 140 amu was applied to each of the reactants (TMS alkynes **7** were assigned a cutoff of 212 amu because the TMS group is cleaved during the synthesis). A molecular weight cutoff of 400 amu and a cLogP of ≤ 3.5 were then applied to the assembled THPs (±)-**1** to (±)-**3** to furnish a virtual library of 4.3 billion compounds; this library would subsequently be available for selection of analogs. To maximize the likelihood of identifying hits with high ligand efficiency for the initial docking screen, we further restricted the molecular weight to 350 amu, resulting in an initial virtual library of 75 million molecules.

Docking & modeling.

Seeking novel ligands for the 5-HT_{2A}R, we used an iterative computational and empirical screening strategy (Figure 1c). We initially did not differentiate between agonists or antagonists, since selective compounds of either class would be useful. As there were no X-ray or cryo-EM structures of the 5-HT_{2A}R available at the time this study was conducted, we first built 1000 homology models templated on the 5-HT_{2B}R X-ray structure bound to LSD, using Modeller (PDB ID: 5TVN, as described in ref. ²¹). The orthosteric ligand LSD was retained during the modeling to ensure a ligand-competent orthosteric binding site. The resulting homology models were evaluated for their ability to enrich 34 known 5-HT_{2A}R ligands from the IUPHAR database²² versus 1899 property matched decoys²³. The models were ranked by their ability to enrich the ligands vs. the decoys, in sensible geometries, among the top scoring docked molecules^{24,25}. Models were also assessed for their ability to reproduce the crystallographic pose of LSD and to form key interactions with the receptor such as the observed salt bridge with Asp^{3.32}.

The best-performing 5-HT_{2A}R model was screened against the 75 million THP library. Each library molecule had an average of 92 conformations calculated for it and was sampled in approximately 23,000 orientations. A total of 7.46 trillion complexes were sampled and scored; the calculation took 8,698 core hours, or just under 9 hours on 1000 cores of our lab cluster. The 300,000 top-ranking docked molecules were clustered by topological similarity using an ECFP4-based Tanimoto coefficient (Tc) > 0.5; this found 14,959 non-redundant clusters. The top-scoring molecules for the top-ranked 4,000 clusters were inspected for unfavorable features, which sometimes are not accounted for by the docking scoring function, including internal ligand strain and the occurrence of unsatisfied ligand hydrogen-bond donors, and for modeled interactions with key binding site residues²⁶. Of those that remained, 205 were filtered for chemical novelty by insisting on ECFP4-based Tc similarities < 0.35 vs. ~28,000 annotated dopaminergic, serotonergic, and adrenergic ligands from the ChEMBL20 database²⁷.

Initial synthesis and testing.

From the remaining top-ranking clusters, we synthesized 17 richly functionalized THPs. The selected primary amines **4** and α,β -unsaturated carbonyls **5** were first condensed to provide α,β -unsaturated imines **8** (Extended Data Fig. 1a). A one-pot reaction sequence then furnished THP sub-types (\pm)–**1** to (\pm)–**3** by Rh(I)-catalyzed C–H addition of imine **8** to alkyne inputs **6** or **7** with *in situ* electrocyclization to give dihydropyridines (DHPs) (\pm)–**9** or (\pm)–**10**, respectively. THPs (\pm)–**1** to (\pm)–**3** were obtained by submitting DHPs (\pm)–**9** or (\pm)–**10** to different reduction protocols without any work-up or isolation. To facilitate the synthesis of some initial compounds, and for later analog synthesis (*vide infra*), a route was developed for the late-stage introduction of various R¹ substituents on the nitrogen of the THP core by preparing THPs (\pm)–**2** to (\pm)–**3** with a cleavable substituent on the nitrogen (Extended Data Fig. 1b). The synthesized THPs display a range of interesting functionalities and are well-differentiated from the endogenous agonist, serotonin, and from previously reported 5-HT_{2A}R synthetic ligands.

The initial set of 17 synthesized THPs were tested in radioligand displacement assays versus the 5-HT_{2A}R, 5-HT_{2B}R and 5-HT_{2C}R subtypes. This identified four molecules with K_i values ranging from 0.67 to 3.9 μ M, a 24% hit rate (Figure 2a–b). In functional assays at the three 5-HT_{2R} subtypes, these four ligands exhibited either agonist or antagonist activity, with agonist activity ranging from 1.9 to 3.0 μ M at the 5-HT_{2B}R (Figure 2c, Extended Data Table 2).

Docked poses of the confirmed ligands suggested that all four interact with conserved binding site residues, including a salt bridge between the THPs' tertiary amine and D155^{3,32}, a characteristic interaction in aminergic and certainly serotonergic²⁸ GPCRs (Figure 2d). Several of the THPs were also predicted to hydrogen bond with N343^{6,55} on TM6 and the main chain of residues on the second extracellular loop (ECL2), and to form van der Waals interactions with residues on transmembrane helices 3, 5 and 6. Since the 5-HT_{2A}R and 5-HT_{2B}R orthosteric binding sites are highly conserved, with only four residues varying between them¹⁶, we hypothesized that even THP ligands binding primarily at the 5-HT_{2B}R subtype could be optimized to engage the 5-HT_{2A}R.

Structure-based optimization.

We initially focused on synthesizing THP analogs that conserved the pyridine and pyrazole substituents at the C5 position, while varying the substituent on the THP nitrogen. This substitution site showed greater variability in the early ligands and is also straightforward to modify from the many available building blocks. Twenty analogs incorporating the pyridine ring at the C5 position were synthesized and assayed for binding, initially as racemates. Several had improved affinity, and even those analogs with reduced affinity provided useful insights into structure activity relationships. Although the 3-hydroxyoxetane functionality was developed as a carboxylic acid bioisostere²⁹, the corresponding carboxylic acid analog (\pm)-**30** had no activity against the 5-HT_{2A}R or 5-HT_{2B}R (Supplementary Figure 2a). However, the oxygen heteroatoms in the hydroxyoxetane do contribute to binding because the 1-methylcyclobutyl (\pm)-**31** and neopentyl (\pm)-**32** analogs had reduced affinity. The location of the basic pyridyl nitrogen is also important as established by the lack of activity of the pyridine regioisomer (\pm)-**33**.

The eight highest affinity racemic analogs were separated by chiral high-performance liquid chromatography (HPLC) and tested for binding and functional activity as single enantiomers (Supplementary Table 2). As exemplified for (**R**)-**35** and (**S**)-**35**, strong chiral discrimination was generally observed for the binding of each pair of enantiomers to both 5-HT_{2A}R and 5-HT_{2B}R. Encouragingly, docking correctly predicted that the *S*-enantiomer would bind with greater affinity. Improved binding affinity and functional activity was observed when the methyl substituent present on the pyridyl ring was replaced by the isosteric but metabolically stable chloro substituent, as exemplified by (**R**)/(**S**)-**35** and (**R**)/(**S**)-**36**. Based upon the incipient 5-HT_{2B}R hit (\pm)-**28** (Extended Data Table 2), the pentyl substituent was introduced on the THP nitrogen of (**S**)-**37**, resulting in sub-micromolar agonist activity at the 5-HT_{2A}R, though still with ~10-fold greater agonism of the 5-HT_{2B}R. Analogues with variable alkyl chain lengths and branching were low nanomolar agonists of the 5-HT_{2B}R, but unfortunately did not improve agonist activity at the 5-HT_{2A}R.

The C5-pyrazole substituent is present in two of our four initial active ligands. To capitalize on this substituent, we revisited the 4.3 billion compound virtual library with molecular weights < 400 amu. Library members with a Tanimoto similarity of > 0.5 to initial hits (\pm)-**26** and (\pm)-**28** were docked to the 5-HT_{2A}R orthosteric binding site and their poses assessed for steric complementarity and for favorable interactions with binding site residues. While numerous substituents with diverse steric profiles and hydrogen bonding abilities were examined off the THP nitrogen ((\pm)-**43**-(\pm)-**54**), in all cases binding affinity of > 10 μ M was observed at the 5-HT_{2A}R (Supplementary Figure 2b). We also experimented with introducing nitrogen substituents from the other initial hit compounds in analogs (\pm)-**55** and (\pm)-**56** but found these changes to be unfavorable. The larger ethyl rather than a methyl substituent, at either C3 ((\pm)-**57**) or on the pyrazole nitrogen ((\pm)-**58**), was not tolerated.

Searching the greater 4.3 billion compound virtual library for similar compounds with heteroaryl groups to replace the pyrazole substituent proved to be more successful, with the azaindole substituent resulting in improved affinity and functional activity. Fourteen azaindole analogs were separated and tested as single enantiomers, with most exhibiting

partial or full agonism at the 5-HT_{2A}R (Supplementary Table 3). Small nitrogen substituents provided the greatest agonist activity and led to the identification of 5-HT_{2A}R strong partial agonists (**R**)-**69** and (**R**)-**70** with 41 nM and 110 nM EC₅₀ values in a calcium flux assay, respectively (Figure 3a–c). In contrast, introduction of the larger 2-(3-(2-methylpyrimidinyl)ethyl) nitrogen substituent provided a selective 5-HT_{2A}R antagonist (**S**)-**65** with 59 nM activity (Figure 3; Supplementary Table 3). The partial agonists (**R**)-**69** and (**R**)-**70** were structurally similar to the initial docking hits, including C5 placement of a heteroaromatic ring and the importance of both unsaturation and the C3 methyl substituent in the THP ring (see 71 and 72).

Target & functional selectivity.

Selective activity on 5-HT_{2A}R versus off-targets like the highly-related 5-HT_{2B}R, other serotonin receptors—metabotropic but also ionotropic—and even transporters is important for usefulness as chemical probes and for therapeutic potential (for instance, 5-HT_{2B}R agonists can cause valvular heart disease)¹⁸. (**R**)-**69** had an agonist EC₅₀ of 190 nM vs. 5-HT_{2B}R, making it 4.6-fold selective for the 5-HT_{2A}R, while (**R**)-**70** is 6.4-fold selective for 5-HT_{2A}R versus 5-HT_{2B}R (Figure 3c); the two compounds were 29 to 51-fold selective versus 5-HT_{2C}R. Against a panel of 318 other GPCRs in a β -Arrestin recruitment assay³⁰, neither (**R**)-**69** nor (**R**)-**70** had measurable agonism, nor did either antagonize the hERG ion channel, a toxicology anti-target, up to 10 μ M (Extended Data Fig. 2a–c). By ligand displacement, no substantial binding was measured at 45 other off-targets (Extended Data Table 3 and Supplementary Table 5). While (**R**)-**69** had modest (0.8 μ M) activity for the serotonin transporter, SERT, (**R**)-**70** had no measurable activity, and neither compound was active versus the DAT or NET transporters. Compared to classic psychedelic 5-HT_{2A}R agonists like LSD, psilocin and DMT³¹, the new agonists are selective against most common serotonergic off-targets (Extended Data Fig. 2d–f). While the EC₅₀ of even (**R**)-**69**, at 41 nM, can seem modest, we note that it is within the range of many in vivo active 5HT_{2A} receptors agonists, including mescaline (4 μ M) psilocin (24 nM), LSD (6.4 nM), and lisuride (17 nM), while its selectivity versus 5HT_{2B} and especially 5HT_{2C} is substantially higher than these classic agonists. Meanwhile, the optimized tetrahydropyridines have unusually high ligand efficiencies, reaching 0.6 kcal/HAC, contributing to the high brain exposure achieved by the molecules and to their in vivo efficacy (below).

Unlike the psychedelic 5-HT_{2A}R agonist LSD, which is arrestin-biased^{16,20,21,32}, the new agonists were G protein biased, activating Gq signaling at mid-nanomolar concentrations with high efficacy while β Arr2 recruitment was only detectable at higher concentrations. To quantify these differential kinetics, we calculated transduction coefficients at each time point for Gq and β Arr2 activities. (**R**)-**69** and (**R**)-**70** displayed stable differences unlike the other tested 5-HT_{2A}R ligands, which had more variable patterns (Extended Data Fig. 3).

Structure prediction and determination by cryo-EM.

Since the S-enantiomer docked better during hit optimization, we sought to refine the docked pose of (**S**)-**69**, as it would be important for further optimization of this series. Starting with the homology model of 5-HT_{2A}R used in the ligand discovery phase, 40 ligand poses were generated. These were clustered into six poses and used as starting

points for 50ns molecular dynamics (MD) simulations. Two stable poses emerged and were used to run retrospective free energy perturbation (FEP)³³ for analogs of (*S*)-**69**, comparing these with experimentally measured binding affinities; the ligand-receptor complex whose relative affinities by FEP corresponded most closely to those of the analogs within this series was chosen as the final predicted pose (Supplementary Figure 3). The pose features a salt bridge with D155^{3.32}, a hydrogen bond with S242^{5.46}, and packing interactions with F222^{6.52} (superscripts refer to the Ballesteros–Weinstein numbering system for GPCR residues, where the first number denotes the helix and the second number indicates the residue position relative to the most conserved residue, defined as X.50³⁴).

To template future compound optimization, understand activity at atomic resolution, and to test the predicted structures, we determined the structure of 5-HT_{2A}R bound to (*R*)-**69** by single particle cryogenic electron microscopy (cryoEM). We used our previously reported strategy¹⁶ in which the 5-HT_{2A}R/miniG_q complex was formed from separately purified receptor in the presence of (*R*)-**69** and miniG_q heterotrimer and further stabilized through the binding of a single-chain variable fragment (scFv16)³⁵. We obtained the cryo-EM structure of the complex at a global nominal resolution of 3.4 Å (Figures 4A and Extended Data Fig 4; Extended Data Table 4).

The high quality cryo-EM density in the 5-HT_{2A}R orthosteric site allowed for unambiguous modelling of (*R*)-**69** (Figure 4d), which was further confirmed through the GemSpot pipeline³⁶. Interactions with the orthosteric site residues include the key salt bridge interaction with D155^{3.32}, and a π -stacking interaction between the azaindole of (*R*)-**69** and F340^{6.52} (Figure 4b and 4c). Multiple additional hydrophobic interactions including V156^{3.33}, V235^{5.39}, W336^{6.48} and F339^{6.51}, also seem to play a role in (*R*)-**69** binding. Although other polar interactions may be present in (*R*)-**69** binding, no hydrogen-bond interaction is observed with the orthosteric site residues S239^{5.43}, S242^{5.46} or S159^{3.36} which are key for LSD and 25CN-NBOH (a *N*-benzyl phenethylamine full-agonist¹⁶) binding, respectively.

The superposition of the docked (*S*)-**69** and experimental (*R*)-**69** bound 5-HT_{2A}R structures reveals good correspondence, with the azaindole groups superimposed almost identically (Figure 4e). The cryo-EM structure shows that the (*R*)-**69** THP ring adopts a slightly different conformation to the computationally predicted one, with the C3 methyl substituent pointing to the extracellular side of the binding pocket. Nonetheless, the key interaction between the THP ring amine and the D155^{3.32} carboxylate is present as designed.

The cryo-EM structure of (*R*)-**69** bound 5-HT_{2A}R/miniG_{q/i} informs comparisons with other 5-HT_{2A}R structures (Extended Data Fig. 5). As with our previously described structure of 25CN-NBOH-bound 5-HT_{2A}R in complex with a G protein (PDB: 6WHA¹⁶), reflecting the activated state of the receptor, the intracellular ends of TM5 and TM6 in the (*R*)-**69** bound 5-HT_{2A}R/miniG_{q/i} adopt an open conformation accommodating the binding of the G protein α -5 helix (Extended Data Fig. 5a). 5-HT_{2A}R - miniG_{q/i} interactions are virtually identical to those described for 25CN-NBOH, supporting the significance of 5-HT_{2A}R residues N107^{2.37}, D172^{3.49}, N317^{6.29}, and N384^{8.47} in hydrogen-bonding with G α_q residues E242^{H5.22}, Y243^{H5.23}, Q237^{H5.17}, and N244^{H5.24}. As was also seen in the other

activated structures, in the **(R)-69**/5-HT_{2A}R/miniG_{q/i} complex residues A321^{6.33}, L261^{5.65}, I177^{3.54}, L325^{6.37}, and V324^{6.36} of 5-HT_{2A}R form a hydrophobic core with L236^{H5.16}, L240^{H5.20}, and L245^{H5.25} of Gα_q. In the complex with **(R)-69**, as in the earlier activated structures, receptor stabilization by G protein binding includes the rearrangement of ICL2 to a well-structured α-helix (Extended Data Fig. 5a).

In the **(R)-69** complex, the “toggle switch” residue W336^{6.48} is in an “upward” conformation that is closer to the inactive LSD bound configuration (PDB: 6WGT¹⁶) versus the “downward” configuration observed in the 25CN-NBOH-bound structure (due to the location of the 25CN-NBOH phenol moiety). Nonetheless, W336^{6.48} is found in the same position in both active structures (Extended Data Fig. 5b) due to the opening of TM6 upon G protein binding with an identical subsequent conformation of the side chain of F332^{6.44} in the PIF (P^{5.50}-I^{3.40}-F^{6.44}) motif. The PIF motif is known to undergo conformational changes upon receptor activation²⁰. Notably, **(R)-69** extends more toward TM5 than does LSD in its complex with the inactive state of 5-HT_{2A}R. As also observed for the 25CN-NBOH-bound structure, the **(R)-69**-complex displays an orthosteric binding pocket that is open to the extracellular side of the receptor (Extended Data Fig. 5c, **top**), while it is more closed in the LSD-bound structure¹⁶. Interestingly, even though **(R)-69** lacks a substituent binding towards the intracellular side of the pocket, a deeper extension of the pocket appears to open between TM3 and TM6 (Extended Data Fig. 5c, **bottom**). Compared to newly-determined x-ray structures of the classic agonists serotonin and psilocin³⁷, which bind relatively high in the orthosteric site of the 5HT_{2A}R, towards its cytoplasmic face, **(R)-69** binds about two-rings deeper in the site, more closely engaging recognition residues such as Phe339, Phe340, and Ser242.

Behavioral pharmacology.

The potency and selectivity of **(R)-69** and **(R)-70** prompted us to investigate their biological activities, as drugs targeting the 5-HT_{2A}R as antagonists are prescribed for psychosis and other psychiatric indications³⁸, while agonists can exert psychedelic, anxiolytic, anti-depressive, and anti-drug abuse actions^{16,39}. There is much interest in finding agonists that retain anti-depressive actions without the hallucinogenic effects of classic psychedelics like LSD and psilocin. Encouragingly, both **(R)-69** and **(R)-70** had substantial brain permeability in mouse pharmacokinetic (PK) studies, with intraperitoneal (i.p.) injections of 10 mg/Kg leading to gross brain C_{max} values of approximately 12 and 35 μM, plasma:brain ratios of 1.09 and 0.11, and brain half-lives of 111 and 28.2 min, respectively for **(R)-69** and **(R)-70** (Extended Data Fig. 6); exposures dosed at 1 mg/Kg remained substantial (Extended Data Fig. 6). These favorable CNS exposures prompted us to monitor head twitch responses (HTRs), classic harbingers of 5-HT_{2A}R engagement and psychedelic drug-like activity^{40,41}. Different doses of both **(R)-69** and **(R)-70** induced very low levels of HTRs and, with the vehicle control, these values were significantly lower than those for the psychedelic LSD (Figure 5a). Moreover, both **(R)-69** and **(R)-70** significantly blocked the HTRs induced by LSD itself. The level of inhibition of LSD-induced HTR by **(R)-69** and **(R)-70** is consistent with what one would expect for competition at the doses used, given the substantially greater potency of LSD. Since activation of the 5-HT_{2A}R can lead to hallucinations⁴², partial blockade of LSD-induced HTRs with **(R)-69** and **(R)-70** further demonstrates

these compounds are unlikely to be psychedelic at these doses. In an additional test for psychedelic-like actions, **(R)-69** and **(R)-70** were found to exert no effects on prepulse inhibition (PPI) relative to LSD (Figure 5b; Extended Data Fig. 7a–b).

Besides finding negligible psychedelic potentials for **(R)-69** and **(R)-70**, we tested whether they would acutely stimulate or inhibit open field locomotion. Responses to both compounds were indistinguishable from the vehicle (Extended Data Fig. 8a–b). Moreover, both compounds blocked LSD-stimulated hyperlocomotion—further demonstrating the absence of motor-stimulating activities. Additionally, behavioral sensitization and conditioned place preference were not evident with the compounds relative to cocaine (Extended Data Fig. 8c–d). Hence, **(R)-69** and **(R)-70** do not possess locomotor-stimulating or reinforcing activity.

Psilocybin and LSD are reported to possess anxiolytic and anti-depressive actions in cancer and other patients^{43–46}. Accordingly, we tested effects of **(R)-69** and/or **(R)-70** in mouse genetic and learned helplessness (LH) models of depressive-like behaviors⁴². Some of these experiments used vesicular monoamine transporter 2 heterozygous (VMAT2 HET) mice, which present with motor-retardation in the open field, anhedonia-like behavior to 1 and 1.5% sucrose solutions, enhanced LH, and augmented stress-induced serum corticosterone levels compared to wild-type (WT) controls. Similarly, in mutants immobility times are increased in the forced swim and tail suspension tests; these immobility times are normalized with the well-known anti-depressants imipramine, fluoxetine (FLX), reboxetine, and bupropion. Responses to **(R)-69** and **(R)-70** and several other drugs were examined 30 min and 24 h post-administration in the VMAT2 HET mice (hashed bars, right of each paired column) and compared to WT mice (solid bars, left of each paired column; Figure 5c–d). Examining the first paired columns (Figure 5c–d), WT mice treated with vehicle had lower immobility times than VMAT2 HETs both acutely and at 24 h, consistent with the depressive-like phenotype of these mutants (significant values between pairs are above the bars in all comparisons). Notably, the enhanced immobility of the VMAT2 HET animals was normalized by acute administration of FLX, 1 mg/Kg **(R)-69**, or 0.5 or 1 mg/Kg **(R)-70**, and it remained at WT vehicle levels 24 h post-administration for both doses of **(R)-69** and **(R)-70**. Thus, in this mouse genetic model both **(R)-69** and **(R)-70** possess anti-depressant-like actions at least over 24 h.

To determine whether the anti-depressant-like activities of **(R)-69** and **(R)-70** were mediated through the 5-HT_{2A}R or 5-HT_{2C}R, we administered the respective antagonists MDL 100907 and SB 242084. Unfortunately, relative to the vehicle control, we found both antagonists decreased immobility on their own in VMAT2 HETs, confounding interpretation of this experiment (Extended Data Fig. 7c–d).

To further investigate anti-depressant actions of **(R)-70**, C57BL/6J mice were tested in LH (Figure 6a). Note, these experiments were not conducted with **(R)-69** owing to reagent limitations. Mice were assigned to foot-shock (FS) and non-FS (NFS) conditions and were given 16 days of training. Subsequently, animals received a single administration (i.p.) of vehicle, 1 mg/Kg **(R)-70**, 1 mg/Kg psilocin, or 10 mg/Kg ketamine and sucrose preference responses, immobility times, and escape behaviors were examined over time, with anxiety-like behaviors evaluated 13 days post-injection. Prior to drug administration during the

pairing of sucrose and water solutions (S-W pairing), FS mice showed a reduced sucrose preference compared to NFS animals (Figure 6b). Hence, FS mice exhibit depressive-like behavior. Post-treatment (days 0–20) no significant effects were observed within days among the NFS mice. Crucially, sucrose preference in FS mice was diminished in the vehicle controls *versus* the **(R)-70** and psilocin groups where anti-depressive-like effects were immediate (acute on day 0) and persisting over 3 days post-injection. Thus, **(R)-70** and psilocin substantially increases sucrose preference among the FS mice. Corresponding effects of ketamine were not apparent until day 1 but were maintained through day 3. By day 8 the levels of sucrose preference in all groups were not statistically different. The reduced sucrose preference in FS animals was not due to decreased fluid intake because they drank larger volumes of the sucrose solution and water than NFS mice prior to treatment, as well as through day 3 post-injection; after day 8 levels of intake were similar between the NFS and FS conditions (Extended Data Fig. 7e).

Relative to sucrose preference, responses to the treatments between and within the FS and NFS conditions were more robust in the tail suspension test. Here, immobility times in NFS-treated mice were comparable across the 18 test days (Figure 6c). By contrast, under the FS condition immobility times were high in vehicle controls relative to the **(R)-70** group and this persisted to day 14. Compared to FS vehicle controls, psilocin and ketamine were efficacious on days 1 and 4, with the psilocin effects lasting to day 9 post-injection. Hence, **(R)-70** appears to have anti-depressant-like activities not only in sucrose preference, but also in tail suspension which persisted over days following a single injection.

Besides depressive-like responses, anxiety-like behavior was examined. In the elevated zero maze, FS mice spent less time in the open areas than NFS mice (Extended Data Fig. 9a). Within the FS condition, vehicle-treated animals spent less time in the open areas than animals given **(R)-70**, psilocin, or ketamine. Additionally, in FS mice the latency to enter the open areas was increased, while motor activities were reduced (Extended Data Fig. 9b–c). Together, these findings suggest the FS mice display anxiety-like behaviors and this is especially apparent in vehicle-treated FS mice.

A key aspect of LH is their performance in escape testing⁴². This behavior was examined as the numbers of escapes and latency to escape just prior to treatment (day –1) (Extended Data Fig. 10a–b). Compared to NFS mice, both escape indices were severely affected in FS mice and they persisted throughout the experiment (i.e., through day 19); no treatment effects were noted within the NFS or FS conditions. Together, these results reveal that treatments at the assigned doses could not overcome the escape decrements in the FS condition. Moreover, this decrement in performance suggests the FS mice may be presenting not only with depressive- and anxiety-like behaviors, but also with posttraumatic stress disorder-like responses. To determine whether the different conditions or treatments were differentially sensitive to foot-shock, all mice were tested for reactivity to this noxious stimulus (Extended Data Fig. 10c). Responses in the FS and NFS animals were similar to the 0 to 0.3 mAmp stimuli; responses to the 0.1 to 0.3 mAmp foot-shock were undifferentiated and higher than those to 0 mAmp. No treatment effects were found. Thus, impairment in escape performance in FS mice cannot be attributed to differential sensitivities to foot-shock.

Discussion

Here we describe a structure-based computational screen of a bespoke, ultra-large virtual library of molecules to find functionally-selective agonists with interesting *in vitro* and *in vivo* activities. Three observations merit particular emphasis. First, a virtual library of 75 million tetrahydropyridines furnished structures underrepresented in a general-purpose make-on-demand library, with >99% of the molecules in the THP library having no equivalent in the general-purpose library, and 96% representing different scaffolds. Docking this library prioritized molecules active against 5-HT₂ receptor subtypes, ultimately leading to potent 5-HT_{2A}R agonists with unusual kinetics for G protein signaling versus arrestin recruitment. Second, the cryo-EM structure of the 5-HT_{2A}R/(**R**)-**69** complex confirms the predicted structure and templates future optimization of this new scaffold. Third, the novelty of (**R**)-**69** and (**R**)-**70** was mirrored in the new biology they conferred, leading to agonists without psychedelic drug-like and locomotor-stimulating actions, typical of classical 5-HT_{2A}R receptor agonists like LSD and psilocin,⁴⁷ but with anxiolytic-like and strong antidepressant drug-like effects in mouse models.

Certain caveats merit airing. Synthetically, the rapid synthesis of highly functionalized, readily diversified scaffolds depends upon facile, convergent, and functional-group-compatible syntheses, limiting the scaffolds suitable for specialized virtual libraries. While the initial docking hit rate for 5-HT₂R subtypes was high, at 24%, the hit rate for 5-HT_{2A}R in particular was lower. While the 5-HT_{2A}R/(**S**)-**69** complex was predicted with high-fidelity to the subsequent cryo-EM structure (Figure 4), this demanded extensive MD and FEP simulations,^{33,48} where docking alone and even pose stability by MD alone⁴⁹ were insufficient. Rather it was the combination of stable MD geometries⁴⁹ with FEP based on those geometries that led to the correct prediction. The unusual phenotype of the new agonists—conferring antidepressant drug-like activity without apparent psychedelic-like activity—may reflect their unusual functional selectivity between G protein and βArr recruitment through the 5HT_{2A} receptor. Admittedly, a role for off-targets, including other 5HT₂ subtypes, and even for active metabolites, cannot be excluded. Finally, while the behavioral activity of the new agonists suggests therapeutic potentials, the current molecules demand more exploration and optimization before they can be considered drug candidates.

These caveats should not obscure the central observations of this study. A virtual library of 75 million THPs explored a functionally-congested scaffold underrepresented in general, unbiased make-on-demand libraries. Docking this virtual library prioritized molecules that well-complemented the 5-HT_{2A}R; their optimization led to strong partial agonists with distinct signaling kinetics. As 5-HT_{2A}R agonists, these molecules are potential leads for the development of therapeutics against disorders that have withstood long-term treatment, including depression, anxiety, and posttraumatic stress disorder. More generally, multiple synthetic strategies⁵⁰ and scaffolds may furnish specialized virtual libraries representing chemotypes unavailable among general make-on-demand libraries. Such focused libraries may illuminate receptors and pharmacologies that have thus far been inaccessible to the community.

Materials and Methods

THP virtual library generation.

The THP libraries were created as follows:

A. Reagent selection.— We searched ZINC for commercially available building blocks to find reagents where we could purchase 250 mg for under \$250, filtering out molecules with incompatible functional groups. For instance, molecules containing alkyne moieties in the amines, anilines, or propenal reagents were eliminated. These compound lists were then manually curated for compatibility with the reaction scheme. We found 1848 anilines, 276 trimethylsilylalkynes, 25 tertiary alkynes and 541 non-tertiary alkynes, 147 propenaldehydes, 283 propenals, and 1890 alkyl-amines. We capped the molecular weight to produce lead-like compounds as follows: TMS alkynes, 222 g/mol, propanals and propenaldydes, 160 g/mol, alkyl amines, anilines, and alkynes, 150 g/mol.

B. Reactions.—The reaction SMARTs used for the reactions are listed in Supplementary Table 1. We used RDKit Version 106_03 for all manipulations. We generated molecules and filtered the list to remove molecules larger than 400g/mol and with calculated logP > 3.5.

C. 3D building.—We built the libraries for docking as described for ZINC15⁵².

Homology modeling.

A homology model of the 5-HT_{2A}R was calculated using the crystal structure of 5-HT_{2B}R in complex with LSD as the template (PDB: 5TVN chain A⁵³). Sequence alignment for construction of 5-HT_{2A}R homology models was generated with PROMALS3D⁵⁴, using sequences of the human 5-HT_{2A}R (Uniprot accession number: P28223), 5-HT_{2B}R (P41595), as well as sequences of all available 5-HT_{2B}R X-ray structures PDB: 4IB4 (chain A)⁵⁵, 4NC3 (chain A)⁵⁶, and 5-HT_{2B}R/LSD complex (5TVN chain A; ⁵³). The alignment was manually edited to remove the amino and carboxy termini that extended past the template structure, and to remove the engineered apocytochrome b562 RIL (BRIL) from the template and the corresponding residues in ICL3 of 5-HT_{2A}R. Based on this alignment, 1000 homology models were built using MODELER-9v15⁵⁷. LSD was retained in the modeling to ensure a ligand-competent orthosteric site. Models were evaluated using DOCK 3.7⁵⁸ for their ability to enrich known 5-HT_{2A}R ligands over property-matched decoys in docking to the orthosteric binding site (below). Decoy molecules share the physical properties of known ligands, but are topologically distinct from them and so that are unlikely to bind, thus controlling the enrichment of molecules by physical properties alone. Thirty-four known ligands with MWs < 350 were extracted from the IUPHAR database⁵⁹, and 1899 property-matched decoys were generated using the DUD-E server⁶⁰. The models were ranked by their adjusted logAUC⁶⁰ and by an enrichment factor at 1% of the docked database (EF_{1%}). Models also had to reproduce the crystallographic pose of LSD in the template structure and form key interactions with the receptor, such as the observed salt bridge with Asp^{3.32}. The best scoring model by ligand enrichment was further optimized through minimization with the AMBER and the GAFF force fields, the latter supplemented with AM1BCC charges⁶¹.

The integrity of the minimized model was assessed by redocking the known ligands and decoy molecules and re-calculating enrichment factors.

Library docking and selection of potential ligands for synthesis and testing.

The modeled orthosteric site of the 5-HT_{2A}R model was screened against the 75 million THP library using DOCK3.7⁵⁸. Parenthetically, DOCK3.7 places pre-sampled ligand conformations into binding sites by superimposing ligand atoms on pseudo-atoms (spheres) in the site. These pseudo-atoms represent favorable positions for individual ligand atoms. Here, 45 matching spheres were used, drawn from the docked pose of LSD. The docked ligands were scored by summing receptor-ligand electrostatic and van der Waals interaction energies and corrected for context-dependent ligand desolvation^{62,63}. Receptor structures were protonated using Reduce⁶⁴. Partial charges from the united-atom AMBER⁶¹ force field were used for all receptor atoms. Potential energy grids for the different energy terms of the scoring function were pre-calculated using AMBER⁶¹ for the van der Waals term and the Poisson-Boltzmann method QNIFFT^{65,66} for electrostatics. Context-dependent ligand desolvation was calculated using an adaptation of the Generalized-Born method⁶². Ligands were protonated with Marvin (version 15.11.23.0, ChemAxon, 2015; <https://www.chemaxon.com>), at pH 7.4. Each protomer was rendered into 3D using Corina (v.3.6.0026, Molecular Networks GmbH; <https://www.mn-am.com/products/corina>), and conformationally sampled using Omega (v.2.5.1.4, OpenEye Scientific Software; <https://www.eyesopen.com/omega>). Ligand atomic charges and initial desolvation energies were calculated as described⁵². In the docking screen, each library molecule was sampled in approximately 23,000 orientations and, on average, 92 conformations. Overall, about 7.46 trillion complexes were sampled and scored; this took 8,698 core hours—or under 9 hours of wall-clock time over 1000 cores. Finally, the best scoring configuration for each docked molecule was relaxed by rigid-body minimization. Over 5 million molecules successfully docked, with ~880,000 receiving an energy score of -30 kcal/mol or better (lower).

Once the screen was completed, the top 300,000 ranked molecules were clustered by the ECFP4-based Tanimoto coefficient (Tc) of 0.5 to reduce redundancy. The best-scoring member was used to represent each of the resulting 14,959 clusters. The 4,000 top-ranking cluster heads were manually inspected for favorable geometry and interactions in Chimera⁶⁷. Topologically diverse molecules that adopted favorable geometries and formed specific interactions with binding site residues, such as a charge interaction with D155^{3,32}, were prioritized. Two hundred and five compounds were selected. These were filtered for novelty by calculating ECFP4-based Tcs against ~28,000 aminergic ligands (acting at serotonin, dopamine and adrenergic receptors) extracted from the ChEMBL20 database⁶⁸. Molecules with Tc < 0.35 to these aminergic ligands were considered as topologically dissimilar and passed this filter. Ultimately, thirty compounds were chosen for synthesis and experimental testing, seventeen of which were successfully synthesized.

(R)-69 binding pose refinement with MD and retrospective FEP.

The 5-HT_{2A}R homology model structure was prepared using the Protein Preparation Wizard (Maestro, Schrodinger, NYC) with the default protocol, and protonation states for histidine, glutamic and aspartic acid residues were predicted by PROPKa⁶⁹ at a pH of 7.4. **(R)-69** was

docked to the prepared structure via Glide SP and Induced Fit Docking (IFD) (Schrodinger, NYC). By enforcing hydrogen bond interactions to D155^{3,32}, three poses were generated from each program and were subjected to Molecular Dynamics (MD) using Desmond.

The Force Field Builder⁷⁰ was used to parametrize missing dihedrals of (**R**)-**69**. Then, each pose of (**R**)-**69** together with the prepared receptor structure was embedded in a POPC membrane, solvated, and had Na⁺ Cl⁻ ions added to a 0.15 mM concentration. The MD systems were equilibrated for 100 ps of Brownian NVT at 10 K with restraints on all the solute's heavy atoms, followed by 100 ps of Brownian NPT at 50 K and 200 ps of NP γ T at 50 K. Then the system was heated from 100 K to 300 K over 300 ps of NP γ T ensemble with gradual release of restraints. A final NVT unrestrained was run for 200 ps. The production runs were sampled for 50 ns of unrestrained NP γ T ensemble at 298 K. Trajectories from the production run were analyzed using Simulation Interaction Diagram for RMSD, RMSF, protein-ligand interactions and ligand torsional profile.

Free Energy Perturbation (FEP) calculations were performed using FEP+ (Schrodinger, NYC)⁷¹ on (**R**)-**69** and 19 analogs. Missing torsional parameters for the ligands were refitted using Force Field Builder⁷⁰. Glide SP docking with tight core constraint was used to align ligands to (**R**)-**69** of the equilibrated system. A perturbation map was then built using cyclohexamine as the custom core. Perturbations in complex and in solvent were sampled in the NP γ T ensemble for 10 ns, and the perturbation map was analyzed using FEP+.

THP synthesis.

Compounds were synthesized as depicted in Extended Data Fig. 1. THPs (\pm)-**1** through (\pm)-**3** were obtained via a one-pot reaction sequence from imines **8** and alkynes **6** or **7** following previously described procedures (Extended Data Fig. 1a)⁷²⁻⁷⁴. All imines were freshly prepared from amines **4** and α,β -unsaturated carbonyls **5**. Select THP compounds were synthesized in two additional steps when the late-stage introduction of various R¹ substituents on the nitrogen of the THP core was desired (Extended Data Fig. 1b). Starting inputs **4-7** that were prohibitively expensive or had long delivery times were also synthesized (details for relevant building blocks are outlined in Supplementary Data 1). Final products were purified by silica gel chromatography, and enantiomerically pure compounds were obtained using chiral high-performance liquid chromatography (HPLC). Identity and purity were confirmed by ¹H and ¹³C NMR and high-resolution mass spectrometry (HRMS). See Supplementary Data 1 for detailed synthetic procedures, analytical data, NMR spectra, and, when appropriate, chiral HPLC traces to demonstrate enantiomeric purity for all final products listed in Extended Data Table 2 and Supplementary Tables 2-3.

Radioligand binding assay.

HEK293T cells were purchased from the American Type Culture Collection (ATCC, ATCC CRL-11268). HEK293T cells were authenticated by the supplier (ATCC) using morphology and growth characteristics, and STR profiling, and tested negative for mycoplasma infection. Competitive binding assays were performed using membrane preparations from HEK293T cells transiently expressing 5-HT_{2A}R, 5-HT_{2B}R, and 5-HT_{2C}R. Binding assays were run in

96-well plates in the standard binding buffer (50 mM Tris, 0.1 mM EDTA, 10 mM MgCl₂, 0.1% BSA, 0.01% ascorbic acid, pH 7.4). Fifty μL each of ³H-LSD (final 0.5 nM) for 5-HT_{2A}R and 5-HT_{2B}R, and ³H-Mesulergine (final 1 nM) for 5-HT_{2C}R, drug solution (3 X), and homogeneous 5-HT_{2A}, 2B and 2C membrane solutions were incubated in 96-well plates in the standard binding buffer. The reaction was incubated for 2 h at room temperature in the dark and terminated by rapid vacuum filtration onto chilled 0.3% PEI-soaked GHF/A filters followed by three quick washes with cold washing buffer (50 mM Tris HCL, pH 7.4) and read. Results were analyzed using the equation 'one-site fit Ki' in GraphPad Prism 9.0.

Calcium flux assay.

Stable cell lines for 5-HT_{2A}R, 5-HT_{2B}R and 5-HT_{2C}R generated using the Flp-In 293 T-Rex Tetracycline inducible system (Invitrogen). Tetracycline-induced cells were seeded in 384-well poly-*L*-lysine plates at a density of 10,000 cells/well in DMEM containing 1% dialyzed FBS at least 16–24 h before the calcium flux assay. On the day of assay, cells were incubated (20 μL/well) for 1 h at 37°C with Fluo-4 Direct dye (Invitrogen) reconstituted in FLIPR buffer (1 X HBSS, 2.5 mM probenecid, and 20 mM HEPES, pH 7.4). After dye loading, cells were placed in a FLIPR^{TETRA} fluorescence imaging plate reader (Molecular Dynamics). Drug dilutions were prepared at 3 X final concentration in drug buffer (1 X HBSS, 20 mM HEPES, 0.1% BSA, 0.01% ascorbic acid, pH 7.4), aliquoted into 384-well plates, and placed in the FLIPR^{TETRA} for drug stimulation. The fluidics module and plate reader of the FLIPR^{TETRA} were programmed to read baseline fluorescence for 10 s (1 read/s), then 10 μL of drug/well was added and read for 5 min (1 read/s). Fluorescence in each well was normalized to the average of the first 10 reads (i.e., baseline fluorescence). Then, the maximum-fold increase, which occurred within the first 60 s after drug addition, was determined and fold over baseline was plotted as a function of drug concentration. Data were normalized to % 5-HT stimulation and analyzed using “log(agonist) versus response” in Graphpad Prism 9.0.

BRET (Bioluminescence Resonance Energy Transfer) assay.

For 5-HT_{2A}R, 5-HT_{2B}R, and 5-HT_{2C}R-mediated G protein activation, HEK293T cells were plated either into 6-well dishes containing 700–800,000 cells/well or into 10-cm dishes at approximately 7–8 million cells/dish. Cells were transfected 2–4 h later, using a 1:1:1 ratio of the receptor:GαRluc8:Gβ:GγGFP DNA⁷⁵. Transit 2020 (Mirus biosciences) was used to complex the DNA at a ratio of 3 μL Transit/μg DNA in OptiMEM (GIBCO) at a concentration of 10 ng DNA/μL OptiMEM. The next day, cells were harvested from the plate using Versene (0.1M PBS + 0.5 mM EDTA, pH 7.4), and plated into poly-*D*-lysine-coated 96-well white assay plates (Greiner) at a density of 25–50,000 cells/well. One day after plating in 96-well plates, white backings (Perkin Elmer) were applied to the clear bottoms of the plate, and the medium was carefully aspirated and replaced with 60 μL buffer (1 X HBBS, 20 mM HEPES, pH 7.4), incubated for 10 min at 37 °C, and incubated again for 10 min but at room temperature. The buffer was carefully aspirated and replaced with 50 μM coelenterazine 400a (nanolight technology) in 60 μL buffer (1 X HBSS, 20 mM HEPES, pH 7.4). After a 5-min equilibration period, cells were treated with 30 μL of 3 X final concentration in drug buffer (1 X HBSS, 20 mM HEPES, 0.1% BSA, 0.01% ascorbic acid, pH 7.4) for an additional 5 min. Plates were read in a LB940 Mithras plate reader

(Berthold Technologies) with 395 nm (RLuc8-coelenterazine 400a) and 510 nm (GFP2) emission filters, at 1 s integration times. Plates were read six times, and measurements from the sixth read were used in all analyses. The BRET ratio represents the ratio of the GFP2 emission to rLuc8 emission. Data were normalized to % 5-HT stimulation and analyzed using nonlinear regression “log(agonist) versus response” in GraphPad Prism 9.0.

To measure 5-HT_{2A}R, 5-HT_{2B}R, and 5-HT_{2C}R-mediated β -arrestin2 recruitment, HEK293T cells were co-transfected in a 1:5 ratio with human 5-HT_{2A,B,C}R containing C-terminal *Renilla* luciferase (Rluc8) and Venus-tagged N-terminal β -arrestin2. After at least 16 h, transfected cells were plated in poly-*L*-lysine coated 96-well white clear bottom cell culture plates in plating media (DMEM + 1% dialyzed FBS) at a density of 25–50,000 cells in 200 μ L/well and incubated overnight. The next day, media were decanted and cells were washed twice with 60 μ L drug buffer (1 X HBss, 20 mM HEPES, 0.1% BSA, 0.01% ascorbic acid, pH 7.4), then 60 μ L of drug buffer was added per well. For kinetic experiments, plates were incubated at 37°C at least 20 min prior to receiving drug stimulation. Afterward, 30 μ L of drug (3 X) was added per well and incubated for the designated time-points. Before reading, 10 μ L of the Rluc substrate, coelenterazine h (Promega, 5 μ M final concentration) was added per well, incubated an additional 5 min to allow for substrate diffusion, and the plates were immediately read for both luminescence at 485 nm and fluorescent eYFP emission at 530 nm for 1s/well using a Mithras LB940 multimode microplate reader. The ratio of eYFP/Rluc was calculated per well and the net BRET ratio was calculated by subtracting the eYFP/Rluc per well from the eYFP/Rluc ratio in wells without Venus- β -Arrestin present. Data were normalized to % 5-HT stimulation and analyzed using nonlinear regression “log(agonist) versus response” in GraphPad Prism 9.0.

GPCRome screen using PRESTO-TANGO.

Screening of compounds using the PRESTO-Tango GPCRome was accomplished using previously described methods with several modifications⁷⁶. Confluent HTLA cells were passaged and subsequently plated in white 384-well clear bottom plates (Greiner) in DMEM (Sigma) with 1% dialyzed FBS and 10 U/mL penicillin-streptomycin (Gibco). After incubating at 37°C and 5% CO₂ for 18 h, the cells were transfected using PEI (Sigma) with an in-plate adapted method⁷⁶. Briefly, 22 ng/well PRESTO-Tango GPCR DNAs were resuspended in OptiMEM (Gibco) and hybridized with PEI prior to dilution and distribution into 384-well plates and subsequent addition to cells. As an experimental control, dopamine receptor D2 was transfected in every plate. After overnight incubation, drugs diluted in DMEM with 1% dialyzed FBS were added to cells without replacement of the medium, and medium alone was added for basal signals. For the tested compounds, a final concentration of 3 μ M was used. Dopamine receptor D2 assay controls were activated with 0.1 mM quinpirole in 16 replicate wells. The remaining steps of the PRESTO-Tango protocol were followed as previously described⁷⁶. Results were presented in the form of fold over basal for each receptor and plotted in GraphPad Prism.

Formation of 5-HT_{2A}R/miniG_{q/i} heterotrimer and scFv16.

The Bac-to-Bac Baculovirus Expression System (Invitrogen) was used to generate high-titer recombinant baculovirus (>10⁹ viral particles/ml), expressed in *sf9* cells, and the proteins

5-HT_{2A}R, miniG_α_q_{iN}/β₁/γ₂, and scFv16 were purified. For purification of 5-HT_{2A}R, thawed insect cell membranes were disrupted in a hypotonic buffer containing 10 mM HEPES (pH7.5), 10 mM MgCl₂, 20 mM KCl, and protease inhibitors containing 500 μM AEBSF, 1 μM E-64, 1 μM Leupeptin and 0.15 μM Aprotinin. Subsequently, soluble and membrane-associated proteins were removed in a high osmotic buffer containing 10 mM HEPES (pH7.5), 1,000 mM NaCl, 10 mM MgCl₂, and 20 mM KCl. Purified membranes were incubated in the presence of ligand, 25 μM (**R**)-**69**, and protease inhibitor cocktail at 4°C for 2 h. The membranes were incubated with 2.0 mg/ml iodoacetamide (Sigma) for 30 min and were solubilized in the buffer containing 50 mM HEPES (pH7.5), 1% (w/v) n-dodecyl-β-D-maltopyranoside (DDM, Anatrace), 0.2% (w/v) cholesterol hemisuccinate (CHS, Sigma) and 150 mM NaCl, at 4°C for 2 h. Solubilized 5-HT_{2A}R proteins in the supernatants were isolated by ultra-centrifugation at 40,000 xg at 4°C for 50 min, and then incubated at 4°C overnight with TALON IMAC resin (Clontech), 800 mM NaCl and 20 mM imidazole as the final buffer concentrations. The resin was washed with 10 column volumes of buffer I containing 50 mM HEPES (pH7.5), 0.1% (w/v) DDM, 0.02% (w/v) CHS, 800 mM NaCl, 10% (v/v) glycerol, 20 mM imidazole and 50 μM (**R**)-**69** and with 10 column volumes of buffer II consisting of 50 mM HEPES (pH7.5), 0.05% (w/v) DDM, 0.01% (w/v) CHS, 500 mM NaCl, 10% (v/v) glycerol and 50 μM (**R**)-**69**. The protein was eluted using 3 column volumes of buffer containing 50 mM HEPES (pH7.5), 0.05% (w/v) DDM, 0.01% (w/v) CHS, 500 mM NaCl, 10% glycerol, 250 mM imidazole and 50 μM (**R**)-**69**. The sample was concentrated in a Vivaspin 20 concentrator with a molecular weight cutoff of 100 kDa (Satorius Stedim) to 500 μL. This volume of 5-HT_{2A}R protein sample was applied to PD MiniTrap G-25 columns (GE Healthcare) to remove imidazole with buffer containing 20 mM HEPES (pH7.5), 100 mM NaCl, 0.5% (w/v) LMNG, 0.05% (w/v) CHS, 0.00025% (w/v) GDN, 100 μM TCEP, and 50 μM (**R**)-**69**. The N-terminal BRIL was removed by addition of His-tagged PresCission protease (GeneScript) with incubation overnight at 4°C. Protease-cleaved BRIL and uncleaved protein were trapped by equilibrated TALON IMAC resin (Clontech) and the flow-through was collected. The 5-HT_{2A}R was further purified by size-exclusion chromatography on a Superdex 200 10/300 gel filtration column (GE Healthcare) with SEC buffer containing 20 mM HEPES (pH 7.5), 100 mM NaCl, 0.001% (w/v) LMNG, 0.0001% (w/v) CHS, 0.00025% (w/v) GDN, 100 μM TCEP, 1 mM MgCl₂, and 25 μM (**R**)-**69**, and stored until use.

For purification of the Gq heterotrimeric complex, insect cells (*sf9*) expressing the miniG_α_q_{iN}/β₁/γ₂ were harvested 72 h post-infection. Cells were lysed in buffer containing 20 mM HEPES (pH 7.5), 100 mM NaCl, 30 mM imidazole, 5 mM β-mercaptoethanol, 1 mM MgCl₂, 0.2% (v/v) Triton X-100 and protease inhibitors, and the soluble fraction was isolated by ultra-centrifugation at 40,000 xg at 4°C for 50 min. The supernatant was incubated with His60 Ni Superflow resin (Takara) at 4°C for 2 h. The Ni-NTA resin was washed with 10 column volumes of buffer containing 20 mM HEPES (pH 7.5), 100 mM NaCl, 30 mM imidazole, and 5 mM β-mercaptoethanol. The heterotrimeric G protein was eluted using buffer containing 20 mM HEPES (pH 7.5), 100 mM NaCl, 300 mM imidazole, and 5 mM β-mercaptoethanol. The PresCission protease (HRV3C protease) was added and the histidine tag was cleaved at 4°C overnight. The histidine tag-cleaved heterotrimeric G protein was further purified by size-exclusion chromatography on a Superdex 200 10/300

gel filtration column (GE Healthcare) with SEC buffer containing 20 mM HEPES (pH 7.5), 100 mM NaCl, 0.001% (w/v) LMNG, 0.0001% (w/v) CHS, 0.00025% (w/v) GDN, and 100 μ M TCEP, and collected and concentrated to ~20 mg/ml and stored at -80°C until use.

The purification process of scFv16 was essentially as previously reported⁷⁷. Media expressing scFv16 from insect cells (*Sf9*) was pH balanced to pH 8.0 by addition of Tris powder. Chelating agents were quenched by addition of 1 mM nickel and 5 mM CaCl_2 and incubated with stirring for 1 h at 25°C . The precipitates were removed by centrifugation at $16,263 \times g$ for 30 min and the supernatant was incubated with His60 Ni Superflow Resin (Takara) for 5 h. The resin was loaded over a Poly-Prep Chromatography column (Bio-Rad) and washed with buffer containing 20 mM HEPES pH7.5, 100 mM NaCl, and 20 mM imidazole. The protein was eluted with buffer containing 20 mM HEPES pH7.5, 100 mM NaCl, and 300 mM imidazole, and treated with PresCission protease to cleave the C-terminal His₈ tag. The cleaved protein was further purified by size-exclusion chromatography using a Superdex 200 10/300 gel filtration column (GE Healthcare). Monomeric fractions were pooled, concentrated, flash frozen in liquid nitrogen and stored at -80°C freezer until use.

Purified 5-HT_{2A}R/(**R**)-**69** was mixed with a 1.2 molar excess of miniG $\alpha_{\text{qiN}}/\beta_1/\gamma_2$ heterotrimer. The coupling reaction was allowed to proceed at 24°C for 1 h and was followed by addition of 0.2 U/mL (final concentration) of apyrase to catalyze the hydrolysis of free GDP. After 1 h, 1–1.5 molar excess of scFv16 was added to the 5-HT_{2A}R and miniG $\alpha_{\text{qiN}}/\beta_1/\gamma_2$ mixture and incubated overnight at 4°C . 5-HT_{2A}R, miniG $\alpha_{\text{qiN}}/\beta_1/\gamma_2$ and scFv16 mixture were further purified by size-exclusion chromatography on a Superdex 200 10/300 column in SEC buffer containing 20 mM HEPES (pH 7.5), 100 mM NaCl, 0.001% (w/v) LMNG, 0.0001% (w/v) CHS, 0.00025% (w/v) GDN, 25 μ M (**R**)-**69**. Peak fractions were concentrated to ~ 17.4 mg/ml for cryo-electron microscopy studies.

Cryo-EM data collection and 3D reconstruction.

A volume of 3.5 μ L of purified 5-HT_{2A}R/miniG α_{qiN} complex bound to (**R**)-**69** at a concentration of ~ 17 mg/mL was applied to glow-discharged (50 s at 10 mA) holey carbon grids (Quantifoil R1.2/1.3) under 100% humidity. Excess sample was blotted away for 3 s at 22°C , and the grids were subsequently plunged-frozen into liquid ethane using a Vitrobot Mark IV (Thermo Fisher Scientific). Cryo-EM imaging was performed on a Titan Krios (ThermoFisher) electron microscope operated at 300 kV with a K3 Summit direct electron detector (Gatan) at a magnification of 57,050 X (0.8521 $\text{\AA}/\text{pixel}$) in counting mode. 5140 movies, dose-fractionated over 50 frames, were recorded with a dose rate of 1.2 $\text{e}/\text{\AA}^2$ (0.05 s/frame for a total dose of 60 electrons/ \AA^2) in super-resolution mode with a defocus range of 0.8–1.8 μm using SerialEM⁷⁸. Cryo-EM data processing was performed with Relion 3.1⁷⁹. Dose-fractionated image stacks were subjected to beam-induced motion correction and dose-weighting with MotionCor2⁸⁰. Contrast transfer function parameters for corrected micrographs were determined using CTFFIND-4.1 in Relion. Particles were selected using the reference-based picking algorithm in Relion. A total of 4,038,793 particles were extracted from the corrected 5140 micrographs. Multiple 2D and 3D classification rounds were performed. A subset of 88,393 particles were subjected to CTF refinement and two

rounds of Bayesian polishing before final refinement and sharpening was applied. The resolution of the final map at the 0.143 FSC threshold was estimated to be 3.38 Å by Mtriage in Phenix and 3.45 Å by Relion 3.1 (Extended data Table 4).

Model building and refinement.

The active-state structure of 5-HT_{2A}R/miniG_{q/i} complex bound to NBOH (PDB: 6WHA⁸¹) was used as an initial model for docking into the EM density map using Chimera⁶⁷. The 5-HT_{2A}R/(**R**)-**69** starting model was subjected to iterative rounds of manual refinement in Coot⁸² and real-space refinement in Phenix⁸³. Model statistics were validated with Molprobit⁸⁴. Final refinement statistics are provided in Table S1. UCSF Chimera⁶⁷ and ChimeraX⁸⁵ were used for map/model visualizations and figure preparation. The (**R**)-**69** pose was corroborated using the GemSpot pipeline⁸⁶.

Subjects.

Adult male and female C57BL/6J (#000664; Jackson Labs, Bar Harbor, ME) or wild-type (WT) and vesicular monoamine transporter 2 (VMAT2) heterozygous (HET) mice were used in the behavioral experiments. Details on the VMAT2 mice have been published⁸⁷. No wild animals were used in these experiments and the present investigations did not involve field studies. The mice were housed 3–5/cage according to sex and genotype in a temperature- (21.1–22.2 °C) and humidity- (42–28%) controlled room on a 14:10 h (lights on at 0600 h) light-dark cycle with food and water provided *ad libitum*. For the learned helpless (LH) experiments, mice that received foot-shock during training were housed individually throughout the study. All experiments were conducted during the light-cycle (anhedonia testing was during the dark cycle) with an approved protocol from the Duke University Institutional Animal Care and Use Committee and were performed in accordance with relevant regulations and ARRIVE guidelines.

Drugs.

The synthesis of (**R**)-**69** and (**R**)-**70** are described above in this manuscript. The (+)-LSD-(+)-tartrate (LSD) and psilocin (NIDA Drug Supply Program, Bethesda, MD) were used as psychedelic controls, while fluoxetine (FLX; Sigma-Aldrich, St. Louis, MO), MDL 100907, and SB 242084 (Bio-Techne Corporation, Minneapolis, MN) were used as controls in the tail suspension test with VMAT2 mice. In the learned helplessness study, psilocin (NIDA Drug Supply Program), and ketamine (Henry Schein, Melville, NY) were used as controls. In the behavioral sensitization and conditioned place preference studies, cocaine (Sigma-Aldrich) was used as a control and its vehicle was water (Mediatech Inc., Manassas, VA). The vehicle for all other drugs/compounds was composed of *N,N*-dimethylacetamide (final volume 0.5%; Sigma-Aldrich, St. Louis, MO) that was brought to volume with 5% 2-hydroxypropoyl-β-cyclodextrin (Sigma-Aldrich) in water (Mediatech Inc.). All drugs were administered (i.p.) in a 5 ml/Kg volume.

Behavioral methods.

The sample sizes for these experiments were determined by past experience. Mice were randomly assigned to different treatment groups, except for learned helplessness (LH)

which is described below. All experiments were conducted in a blinded manner; the statistical analyses were dummy coded and annotated subsequently so that the outputs were interpretable. The individuals who conducted the experiments were different from the people who statistically analyzed the data. In addition, the **(R)-69** and **(R)-70** were given labels different from these names. *Open field*: This apparatus has been described⁸⁷. C57BL/6J mice were placed into the open field for 30 min, injected with vehicle, 1 or 3 mg/Kg **(R)-69** or **(R)-70**, or 0.3 mg/Kg LSD, and returned to the open field for 30 min. For LSD blockade, 1 or 3 mg/Kg **(R)-69** or 3 mg/Kg **(R)-70** were administered and the mice were placed into the open field. After 30 min they were removed and injected with LSD and returned to the open field for 30 min. Locomotion was monitored using Fusion Integra software (Omnitech, Columbus, OH) and expressed as distance traveled. N=8 mice for 1 mg/Kg **(R)-69** + 0.3 mg/Kg LSD; N=9 mice for 0.3 mg/Kg LSD; N=10 mice for vehicle, 1 or 3 mg/Kg **(R)-69**, 1 mg/Kg **(R)-70**, 3 mg/Kg **(R)-69** + 0.3 mg/Kg LSD, or 3 mg/Kg **(R)-70** + 0.3 mg/Kg LSD; and N=11 mice for the 3 mg/Kg **(R)-70** treatments. *Head twitch responses*: These behaviors were filmed during the open field studies over the 30 min interval immediately following drug administration. Head twitch responses were scored by individuals blinded to the treatments of the mice. The numbers of mice used in each treatment group are provided in the open field experiment above. *Prepulse inhibition*: This test and apparatus have been described⁸⁸. C57BL/6J mice were administered the vehicle, 1 or 3 mg/Kg **(R)-69** or **(R)-70**, or 0.3 mg/Kg LSD. N=8 mice for LSD; N=9 mice for 1 mg/Kg **(R)-69**; N=11 mice for 3 mg/Kg **(R)-70**; and N=12 mice for the vehicle, 3 mg/Kg **(R)-69**, or 1 mg/Kg **(R)-70** treatments. *Conditioned place preference*: This test and apparatus have been described⁸⁹ and C57BL/6J mice were administered the vehicle, 3 mg/Kg **(R)-69** or **(R)-70**, or 20 mg/Kg cocaine. N=9 mice administered the vehicle and 3 mg/Kg **(R)-69**, the vehicle and 3 mg/Kg **(R)-70**, or the vehicle and cocaine pairings. *Behavioral sensitization*: The apparatus has been described⁹⁰. C57BL/6J mice were placed into the open field for 1 h to collect baseline activity. They were removed, injected with 3 mg/Kg **(R)-69** or 20 mg/Kg cocaine, and returned to the open field for 2 h. This procedure was repeated over 5 consecutive days. A 7 day hiatus was imposed, and the mice were challenged with the same compound and psychostimulant on day 11. Locomotor activity was monitored using Fusion Integra software (Omnitech) and expressed as distance traveled. N=10 mice injected with 3 mg/Kg **(R)-69** or 20 mg/Kg cocaine. *Tail suspension*: The apparatus and procedure have been described⁴². VMAT2 mice received the vehicle, 20 mg/Kg FLX, 0.5 or 1 mg/Kg **(R)-69** or **(R)-70**. Thirty-min later VMAT2 mice were tested in tail suspension over 6 min and were tested again 24 h post-injection. For WT mice: N=9 mice given 20 mg/Kg FLX, 0.5 or 1 mg/Kg **(R)-69**; and N=10 mice that received vehicle, 0.5 or 1 mg/Kg **(R)-70**. For VMAT HET mice: N=9 mice for 20 mg/Kg FLX, 0.5 or 1 mg/Kg **(R)-69**; N=10 mice for 0.5 or 1 mg/Kg **(R)-70**, and N=11 mice for vehicle injections. In a separate experiment with VMAT2 mice, effects of the 5-HT_{2A}R (MDL 100907) and the 5-HT_{2C}R (SB 242084) antagonists were examined as described above. For WT mice: N=8 mice given 1 mg/kg SB; and N=10 mice injected with vehicle or 0.5 mg/Kg MDL. For HET mice: N=9 mice that received 1 mg/kg SB; and N=11 mice were administered vehicle or 0.5 mg/Kg MDL. C57BL/6J mice that were used in the LH study were tested as described above on day 0 at 30-min after injection (day 0) and on days 1, 4, 9, 14, and 18 post-injection (Figure 6a). For the LH experiment: non-foot-shock (NFS) condition – N=9 mice were administered 10

mg/Kg ketamine; and N=10 mice were given vehicle, 1 mg/Kg (**R**)-70, or 1 mg/Kg psilocin. For the foot-shock (FS) condition – N=9 mice for vehicle; N=10 mice for 1 the mg/Kg (**R**)-70, 1 mg/Kg psilocin, or 10 mg/Kg ketamine treatments. *Learned helplessness (LH)*: The apparatus has been described⁴². C57BL/6J mice were assigned to the foot-shock (FS) or non-foot-shock (NFS) conditions and were individually or group housed, respectively, for the duration of the experiment (Figure 6a). Mice were habituated to the apparatus on days –19 and –18. At the end of all sessions, mice were returned immediately to their home-cages. On days –17 to –9, NFS mice explored the apparatus for 60 min; FS animals also had access to the apparatus but were administered 360 0.15 mA foot-shocks for 2 s (10 s variable inter-trial interval or ITI) each day. On day –8 mice in the FS condition were tested in shock escape (0.15 mA foot-shock) for 10 trials (30–90 s ITI) as described⁴². From days –7 to –2, mice in the FS condition resumed LH training; NFS mice continued to explore. The FS mice were randomly exposed to wet bedding and food restriction throughout training. On day –1, animals in the NFS and FS conditions were given 10 trials of shock escape testing. According to their performance in shock escape and sucrose preference testing (see below), they were assigned to 4 treatments: vehicle, 1 mg/Kg (**R**)-70, 1 mg/Kg psilocin, or 10 mg/Kg ketamine and administered these treatments on day 0. On post-injection days 3, 7, 11, 15, and 19 all mice were tested in shock escape for 10 trials. The numbers of successful escapes and latencies to escape were determined by MedAssociates software (St. Albans, VT). The numbers of C57BL/6J mice used in each condition and treatment group are provided in the tail suspension experiment above. *Sucrose preference*: The outline of the procedure has been described⁴². The mice in the LH study were given water-water (W-W) pairings on days –7 to –5 and, once intake was stable, it was followed with a 0.6% sucrose-water (S-W) pairings on days –4 to –2. W-S pairings were resumed on days 0, 1, 3, 8, 16, and 20 post-injection (Figure 6a). The position of the sucrose bottle was alternated over days and the total volume consumed over the 2-h period was recorded. Preference for sucrose was calculated as the volume of sucrose consumed minus the volume of water, divided by the total intake volume, yielding a ratio from –1 to +1. Positive scores indicated a preference for sucrose, negative scores a preference for water, and scored approaching “0” representing no preference for sucrose or water. The numbers of C57BL/6J mice in this experiment are presented in the tail suspension section above. *Elevated zero maze*: This test and apparatus have been described³². The LH mice were tested on day 13 after drug administration (Figure 6a). The numbers of mice in this experiment are presented in the tail suspension section above. *Foot-shock sensitivity*: This test and apparatus have been described⁹¹. The reactivity to foot-shock was tested using intensities of 0, 0.1, 0.2, and 0.3 mAmp on day 21 after drug administration (Figure 6a). N=10 mice/intensity.

Statistics for behavioral studies.

Statistical analyses were performed with IBM SPSS Statistics 27 and 28 programs (IBM, Chicago, IL). The data are presented as means and standard errors of the mean (s.e.m.). As no sex effects were detected, this variable was collapsed in our statistical analyses. All measurement were taken from discrete raw data and, in certain cases, from repeated observations within the same animal (i.e., RMANOVA). One- or two-way ANOVA, repeated measures ANOVA (RMANOVA), or analysis of covariance (ANCOVA) were used (all tests were 2-tailed and normally distributed), followed by Bonferroni corrected pair-wise

comparisons. A $p < 0.05$ was considered significant. The numbers of mice in each group represent the number of replicates for a given experiment. All behavioral results are plotted using GraphPad Prism (San Diego, CA). All primary statistics can be found in Supplementary Table 4.

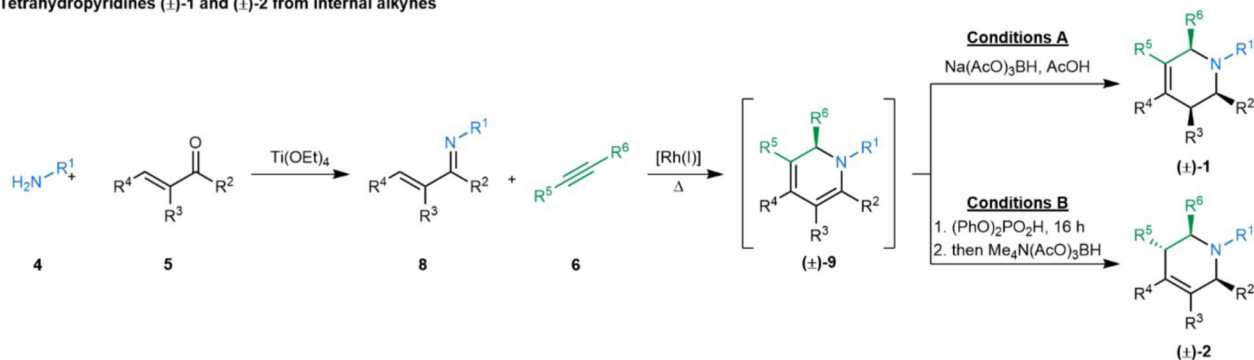
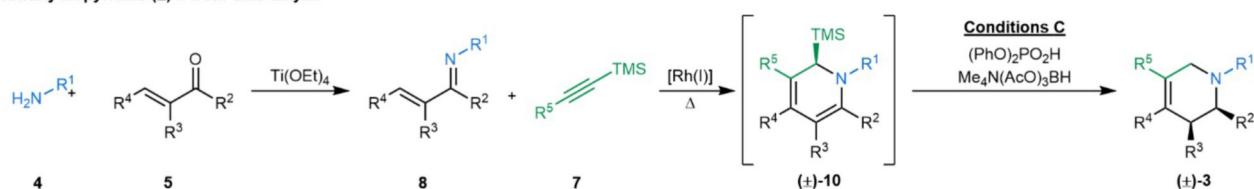
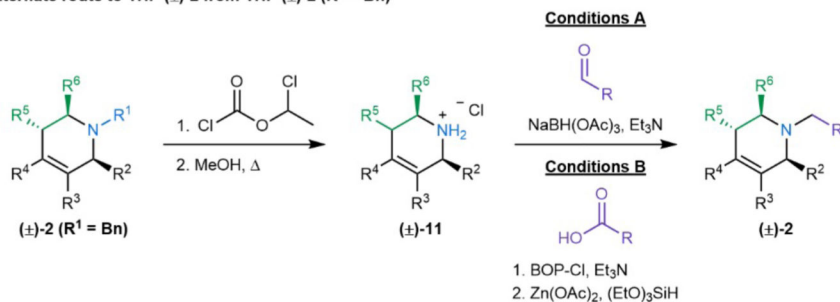
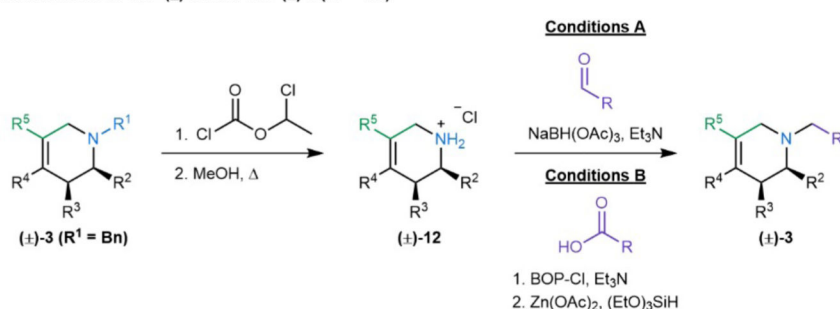
Data Availability Statement:

The cryo-EM density map and corresponding coordinates for 5-HT_{2A}R in complex with the new docking hit (**R**)-**69** have been deposited in the Electron Microscopy Data Bank (EMDB) and the Protein Data Bank (PDB), respectively, under the following accession codes: EMDB entry ID EMD-24378 and PDB entry ID 7RAN. The full THP library of compounds may be freely accessed at <http://thp.docking.org/>. All active compounds are available from the authors upon request. Sequences used to generate the 5-HT_{2A}R homology model are available from the Uniprot database (<https://www.uniprot.org>, accession numbers: P28223, 5P41595, or from the PDB (<https://www.rcsb.org>, accession codes: 4IB4 (chain A), 4NC3 (chain A), 5TVN (chain A)). Figures with associated raw data include Figs. 2 and 3, the underlying activities are uploaded in an Excel file; Fig. 4, Extended Data Figs. 4 and 5: electron density maps and associated files are deposited with the PDB; Fig. 5, underlying numbers are uploaded in an Excel file; Extended Data Figs. 2, 3 and 6, underlying activities are uploaded in an Excel file; Extended data table 3, underlying numbers are supplied in supplementary table 5. Supplementary Fig. 3, underlying numbers are uploaded in an Excel file. Further underlying data are provided in Extended Data Table 4 (cryoEM data collection, refinement & validation), Supplementary Data 1 (synthesis procedures for active compounds, chemical purity of active ligands, spectra and 3D crystallographic structures), and Figures 5 and 6. Extended Data Figures 7–10 depict the raw data points with means and SEMs (Prism files; GraphPad Software, San Diego, CA) and the Supplementary Table 4 displays the statistics from behavioral data (IBM SPSS, versions 27 and 28). All raw behavioral data are uploaded in Excel files.

Code Availability:

DOCK3.7 is freely available for non-commercial research at <http://dock.compbio.ucsf.edu/DOCK3.7/>. A web-based version is freely available to all at <http://blaster.docking.org/>.

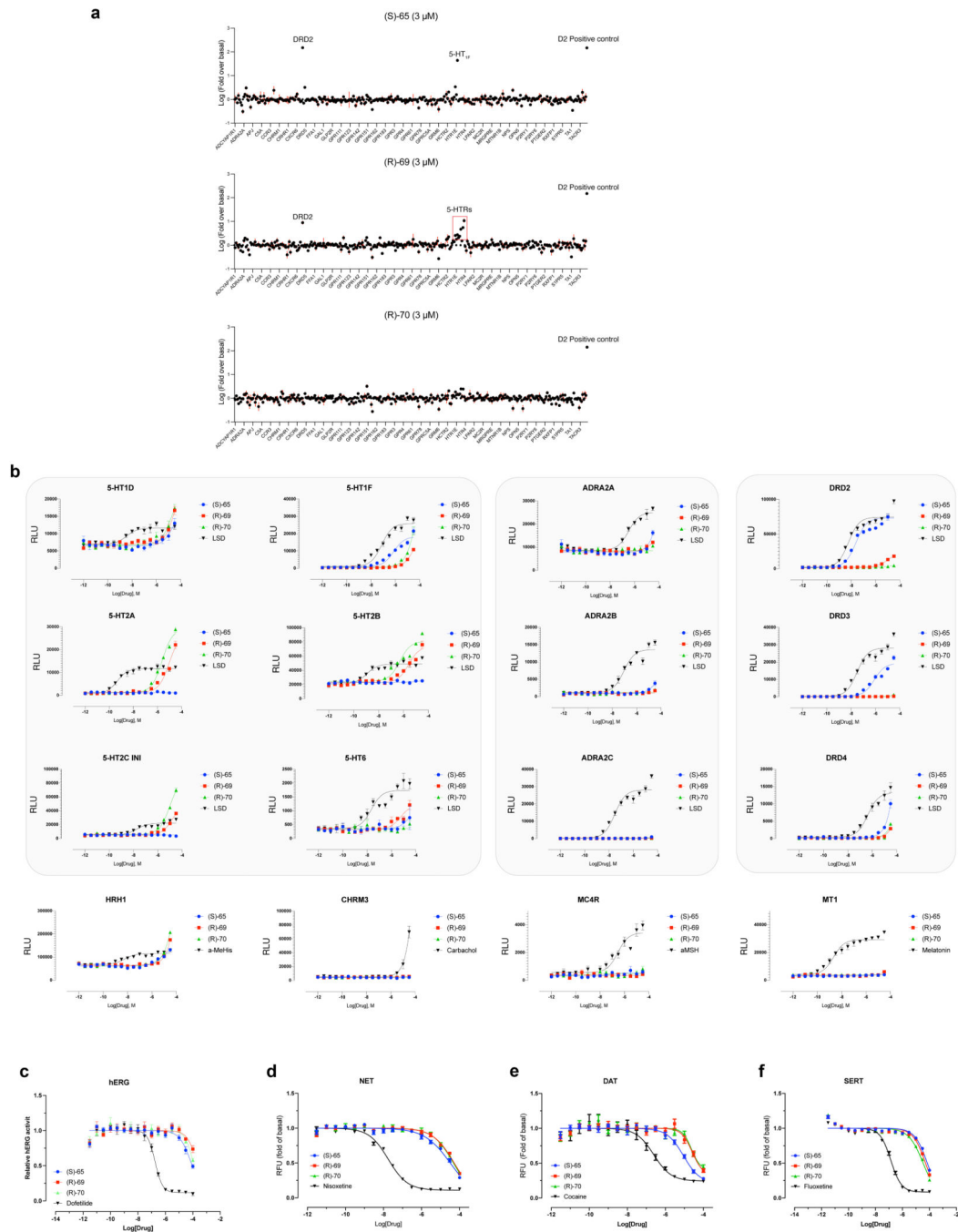
Extended Data

a Tetrahydropyridines (\pm)-1 and (\pm)-2 from internal alkynesTetrahydropyridine (\pm)-3 from TMS alkyneb Alternate route to THP (\pm)-2 from THP (\pm)-2 ($\text{R}^1 = \text{Bn}$)Alternate route to THP (\pm)-3 from THP (\pm)-3 ($\text{R}^1 = \text{Bn}$)

Extended Data Figure 1. (A) Synthetic routes to access densely functionalized, diastereoselective tetrahydropyridines 1 to 3.

Building blocks used for tetrahydropyridines (\pm)-1 and (\pm)-2: R^1 , R^5 , R^6 = alkyl, aryl, heteroaryl; R^2 = H, alkyl; R^3 , R^4 = H, alkyl, aryl, heteroaryl. Building blocks used for tetrahydropyridines (\pm)-3: R^1 = alkyl; R^5 = alkyl, aryl, heteroaryl; R^2 = H, alkyl; R^3 , R^4 = H, alkyl, aryl, heteroaryl. See Supplementary Data 1 for detailed reaction conditions and

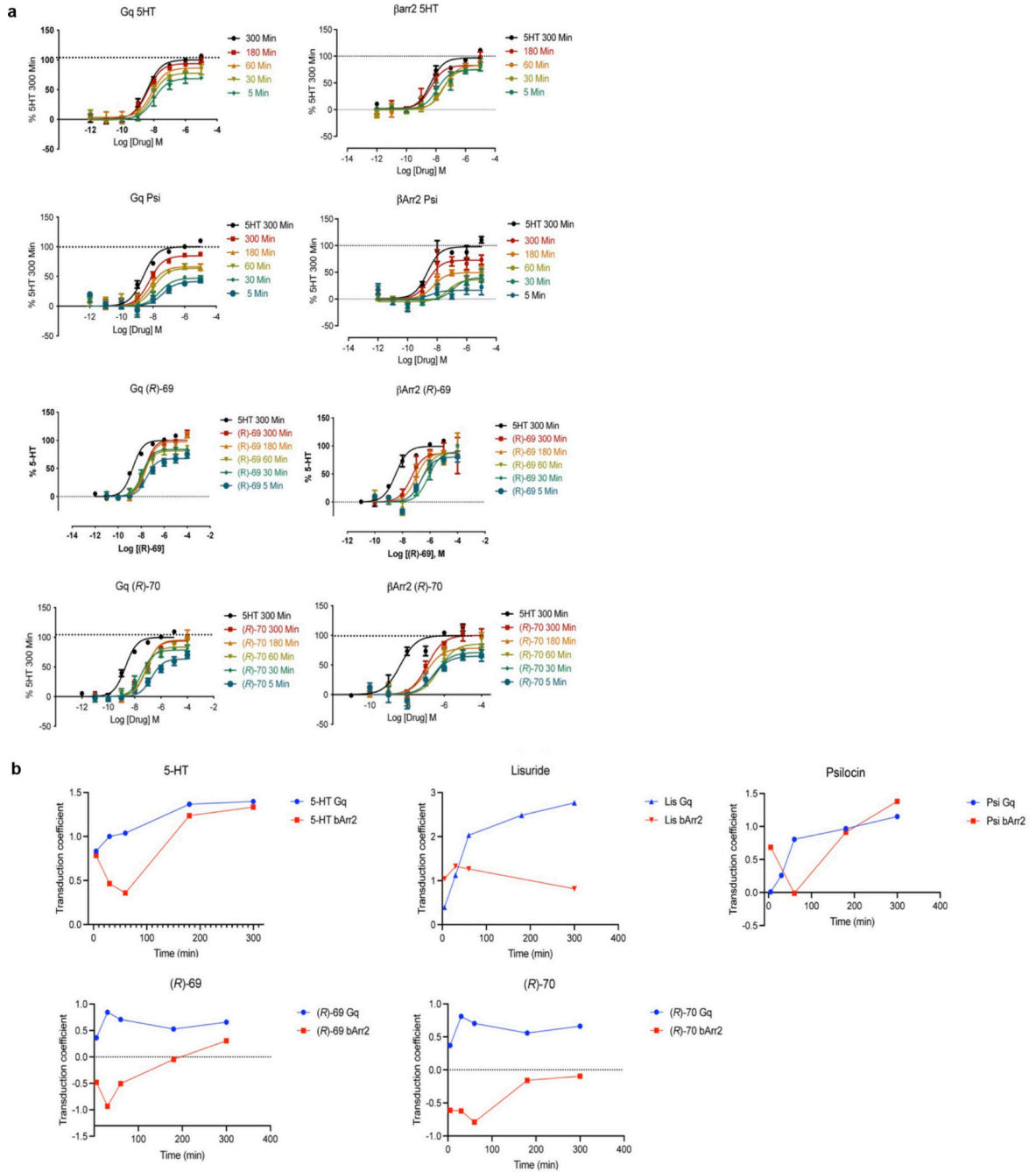
procedures. **(B) Alternate routes for installation of R¹ substituent.** See Supplementary Data 1 for detailed reaction conditions and procedures.



Extended Data Figure 2. Pharmacological profiles of (S)-65, (R)-69, and (R)-70.

(A) Screening of (S)-65, (R)-69, and (R)-70 across the GPCRome (320 receptors) using the PRESTO-Tango platform⁵² with agonists present at 3 μ M concentrations; for viewability, only 1-in-4 receptors are listed on the x-axis. **(B)** Analysis of the function of (S)-65, (R)-69, and (R)-70 on various receptors shows the diverse profiles for each receptor. **(C)-(F)**

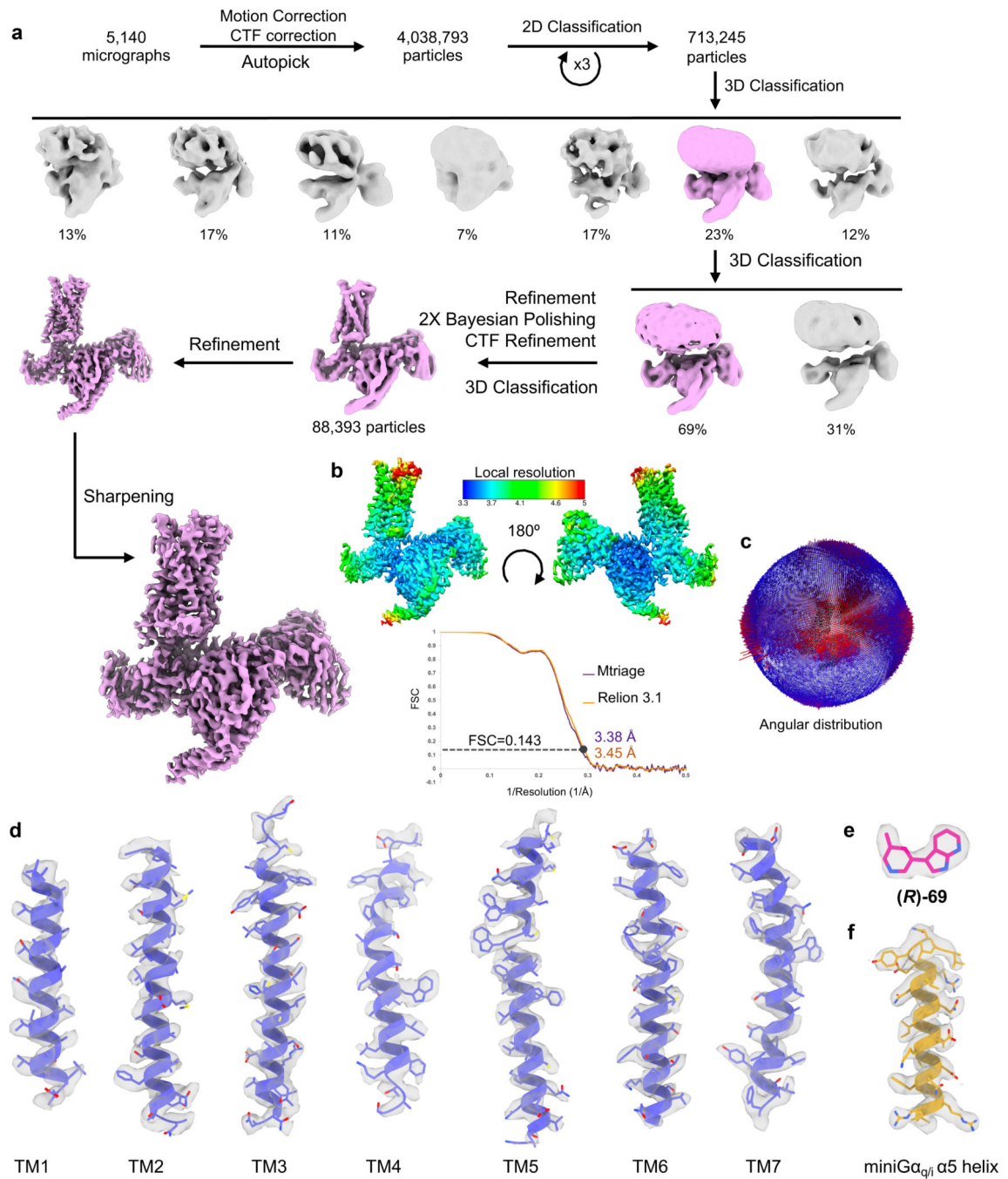
Binding profiles of (S)-65, (R)-69, and (R)-70 on (C) hERG; human ether-a-go-go-related gene, (D) NET; norepinephrine transporter, (E) DAT; dopamine transporter, and (F) SERT; serotonin transporter. Data in (A), (B), (C), (D), (E) and (F) represent the mean ±S.E.M from n=3 independent experiments.



Extended Data Figure 3. Characterization and time course activities of functional bias of (R)-69 and (R)-70 at the human 5-HT_{2A}R.

(A) BRET (Gq dissociation and β -Arrestin 2 association) activities of 5-HT (top panel), psilocin (2nd panel), (R)-69 (3rd panel) and (R)-70 (bottom panel) on the 5-HT_{2A}R. Data

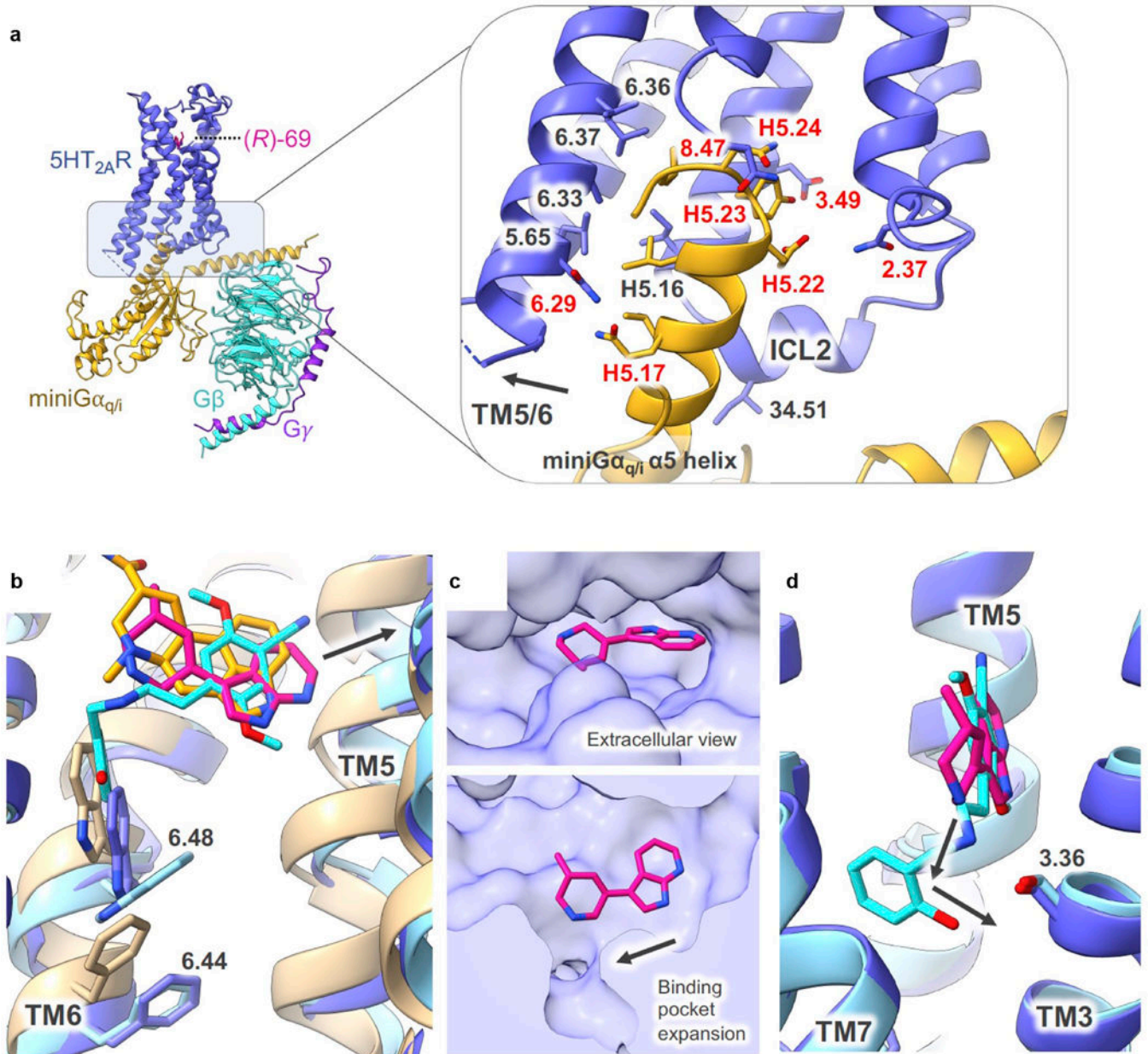
represent the mean \pm SEM from $n=3$ independent experiments, each performed in triplicate. **(B)** Transduction coefficients for Gq and β Arr2 at various time points. Transduction coefficients were measured (see METHODS) for each time point in **(A)** and then plotted vs time.



Extended Data Figure 4. CryoEM workflow.

(A) Workflow of cryo electron microscopy (cryo-EM) data processing of the 5-HT_{2A}R/miniGα_{q/i} complex bound to (R)-69. **(B)** Local resolution estimation heat map and gold

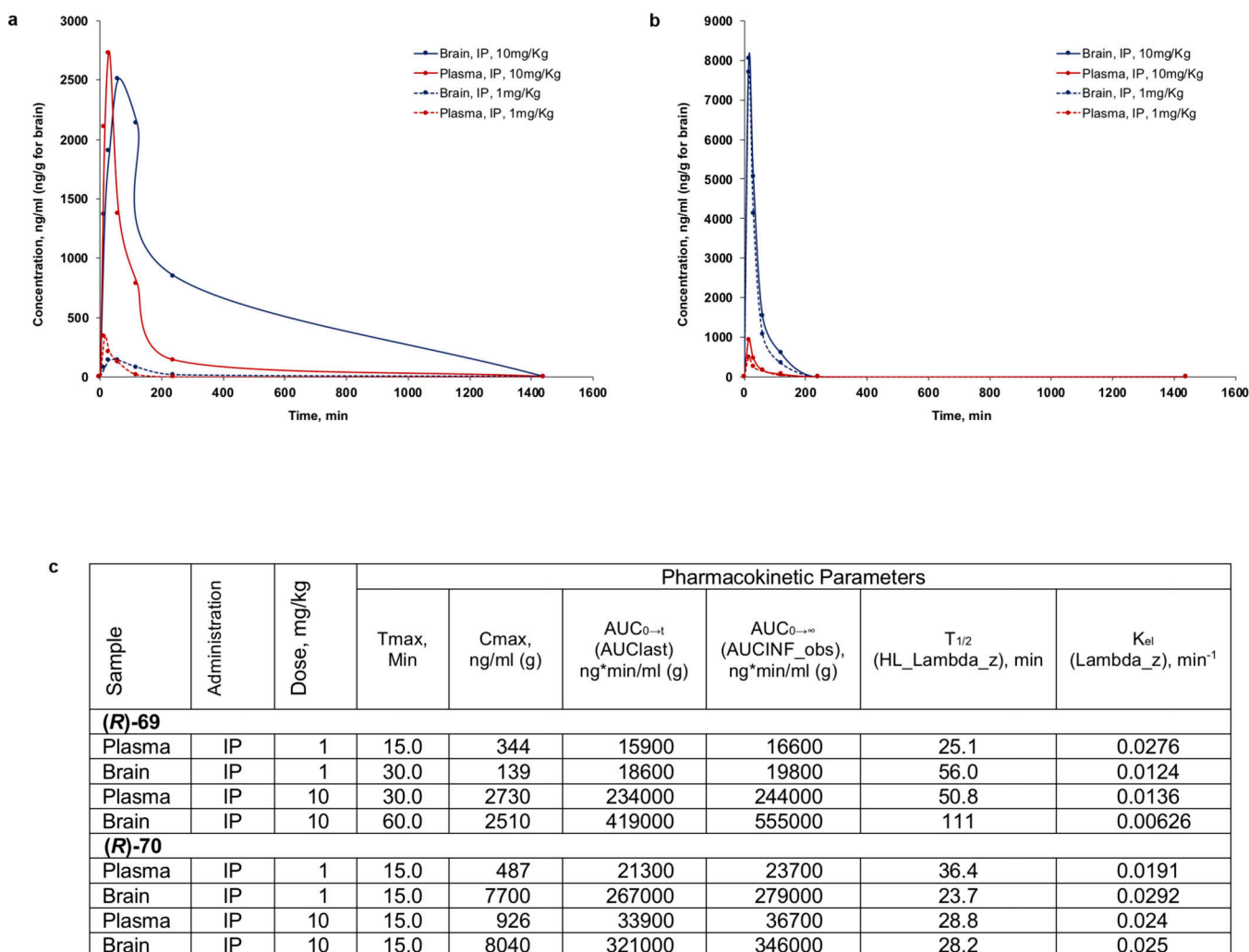
standard Fourier shell correlation (FSC) curve. Dashed line represents the overall nominal resolution at 0.143 FSC of 3.38 Å calculated using Phenix Mtriage and 3.45 Å calculated by Relion 3.1 after post-processing. (C) Angular distribution heat map of particles for cryo-EM reconstruction. (D) Cryo-EM density for TM1–7 of 5-HT_{2A}R, E, (**R**)-69 and F, α 5 helix of miniG $\alpha_{q/i}$.



Extended Data Figure 5: Comparison between the cryo-EM structure of (R**)-69 bound 5-HT_{2A}R/miniG $\alpha_{q/i}$ and other 5-HT_{2A}R structures.**

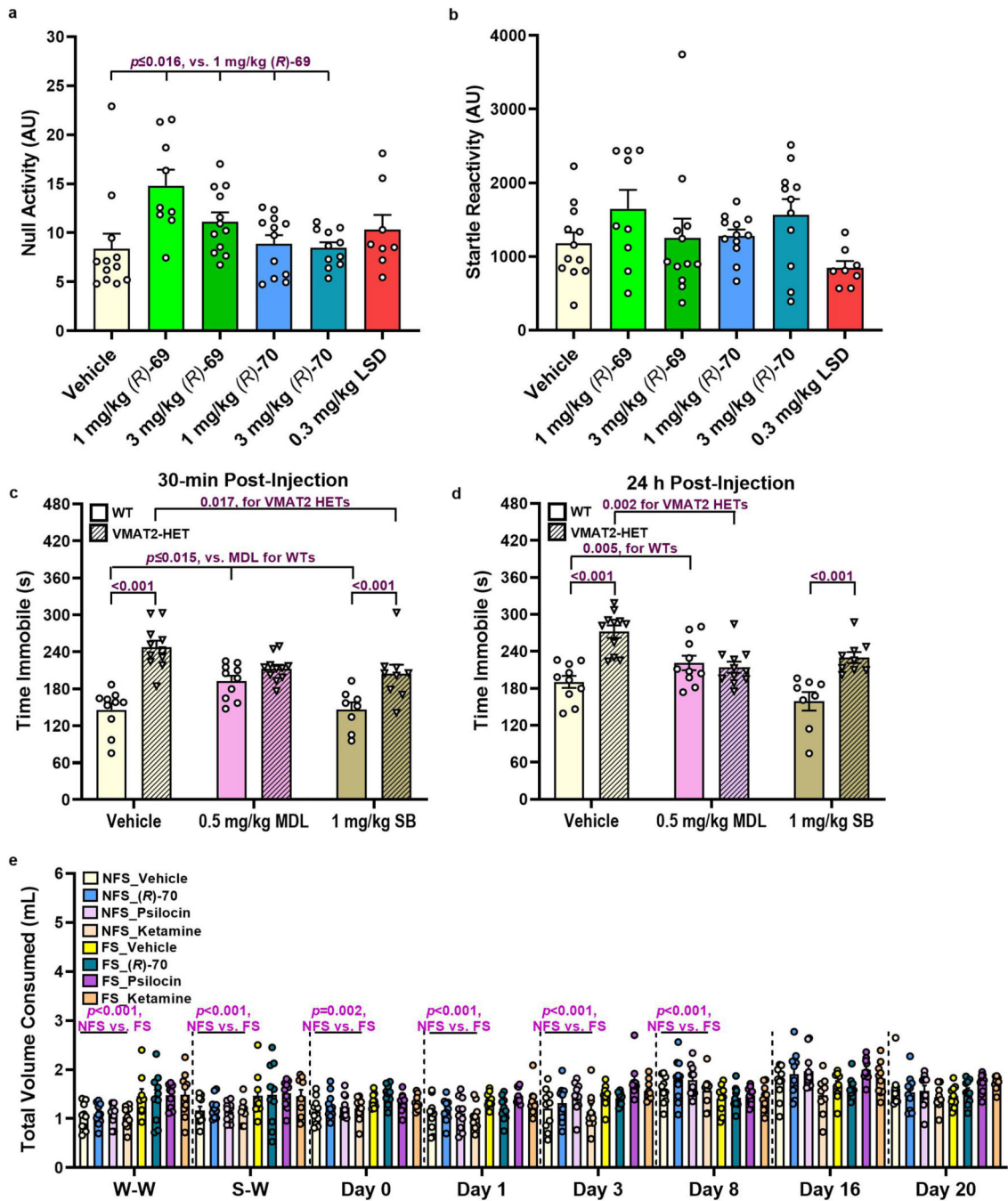
(A) 5-HT_{2A}R - miniG $\alpha_{q/i}$ complex interactions. Arrow points to opening of TM5/6 in active (**R**)-69 bound 5-HT_{2A}R state. (**R**)-69 bound 5-HT_{2A}R in blue; miniG $\alpha_{q/i}$ in gold. Residues involved in hydrophobic interactions are labeled in grey while residues involved

in H-bond interactions are labeled in red. **(B)** Ligand specific interactions with 5-HT_{2A}R. **(R)-69** in magenta. LSD bound 5-HT_{2A}R structure in tan; LSD in orange. 25CN-NBOH bound 5-HT_{2A}R structure in light cyan; 25CN-NBOH in cyan. Arrow points to extension of **(R)-69** and 25CN-NBOH towards TM5. **(C)** Top: view of the 5-HT_{2A}R ligand-binding pocket from the extracellular side; bottom: expansion of binding pocket of 5-HT_{2A}R bound to **(R)-69** towards the cytosolic side of the receptor. **(D)** Proposed optimization of **(R)-69** to engage in a hydrogen-bond interaction with S159^{3.36}. In all panels the Ballesteros-Weinstein numbering is shown in superscript for each residue.



Extended Data Figure 6: Pharmacokinetic analysis of (R)-69 and (R)-70.

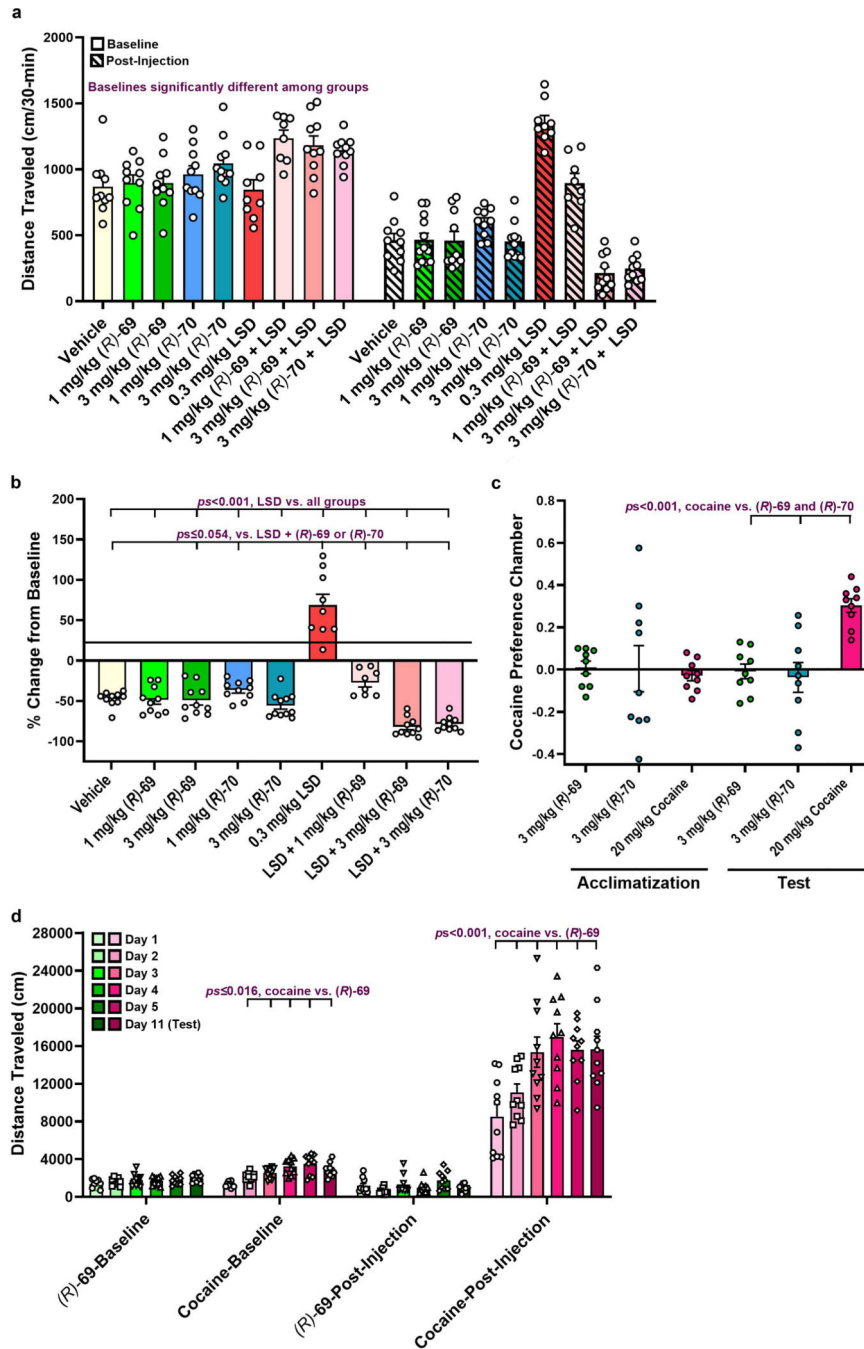
Concentration-time curves for **(R)-69** **(A)** and **(R)-70** **(B)** in male C57BL/6N mice following IP dosing of either 1 or 10 mg/Kg of the compounds. **(C)** Selected pharmacokinetic parameters for **(R)-69** and **(R)-70** in male C57BL/6N mice.



Extended Data Figure 7. Null activity, startle reactivity, anti-depressant-like actions of MDL 100907 and SB 242084, and total volume of sucrose and water consumed.

(A) Null activity during PPI for C57BL/6J mice treated (i.p.) with vehicle, 1 or 3 mg/Kg (R)-69, 1 or 3 mg/Kg (R)-70, or 0.3 mg/Kg LSD. Null activity increases with 1 mg/Kg (R)-69 group. (B) Startle reactivity during PPI with C57BL/6J mice undergoing the same treatments. No significant effects are found. (C) Immobility in tail suspension at 30 min and 24 h with WT and VMAT2 HET mice after a single injection (i.p.) of vehicle, 0.5 mg/Kg MDL 100907, or 1 mg/Kg SB 242084. Genotype differences are observed in acute and

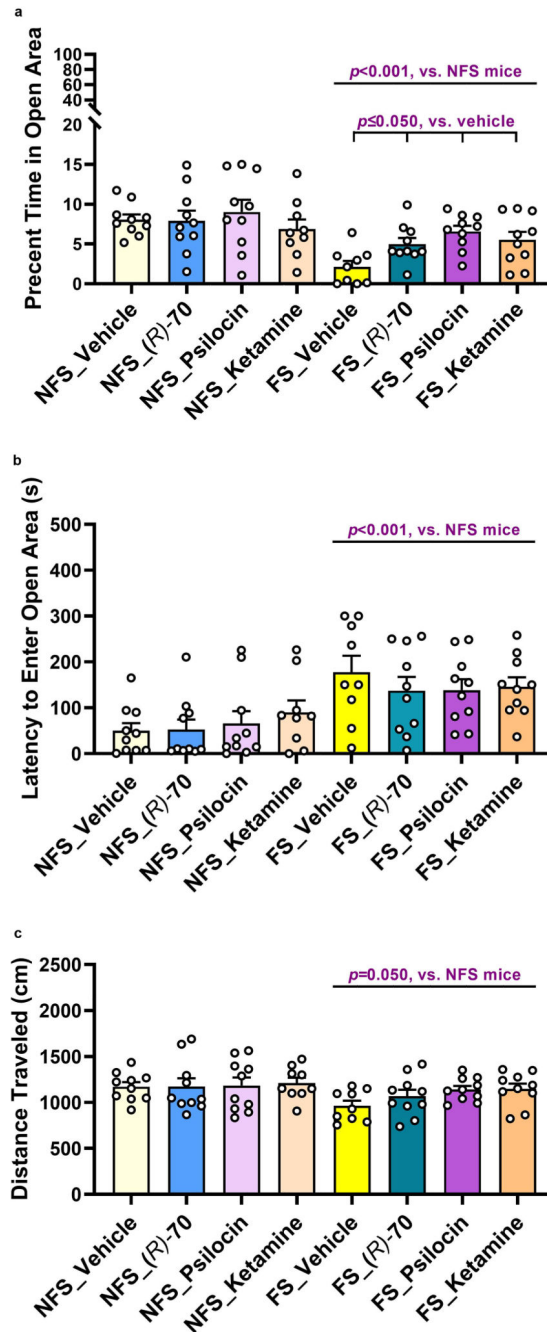
24 h tests with vehicle and SB. In WT mice, immobility is increased acutely with MDL compared to vehicle and SB. The difference between the MDL and vehicle groups persists at 24 h. In VMAT2 HETs, immobility times in vehicle controls are high acutely relative to SB, with a trend ($p=0.055$) for MDL. At 24 h, immobility times for vehicle-treated mice are higher than for MDL. (E) Total fluid consumed during the sucrose preference test with non-foot-shocked (NFS) and foot-shocked (FS) C57BL/6J mice given (i.p.) vehicle, 1 mg/Kg (R)-70, 1 mg/Kg psilocin, or 10 mg/Kg ketamine. FS mice drink more than NFS animals during water-water (W-W) and sucrose-water (S-W) pre-test pairings, as well as on post-injection days 0, 1, and 3. Results presented as mean \pm s.e.m., Ns are found in Methods. Primary statistics are in Supplementary Table 4. In the figure the Bonferroni pair-wise corrected p -values (ps) across multiple comparisons for 1 mg/kg (R)-69 or MDL showing the value closest to $p<0.05$ (respective panels A, C) or within a single comparison (p) from the vehicle, MDL, or SB groups (panels C-D), or condition (panel E).



Extended Data Figure 8. Spontaneous locomotion, conditioned place preference (CPP), and behavioral sensitization to (R)-69 and (R)-70.

(A) Baseline (30 min) and post-injection locomotion (30 min) in C57BL/6J mice after administration (i.p.) of vehicle, 1 or 3 mg/Kg (R)-69, 1 or 3 mg/Kg (R)-70, 0.3 mg/Kg LSD, 1 or 3 mg/Kg (R)-69 + 0.3 mg/Kg LSD, or 3 mg/Kg (R)-70 + 0.3 mg/Kg LSD. Since baseline activities are different among groups, the data are analyzed as percent baseline in the next panel. (B) Percent change from baseline from mice in the same experiment. Compared to vehicle, different doses of (R)-69 or (R)-70 have neither stimulatory nor

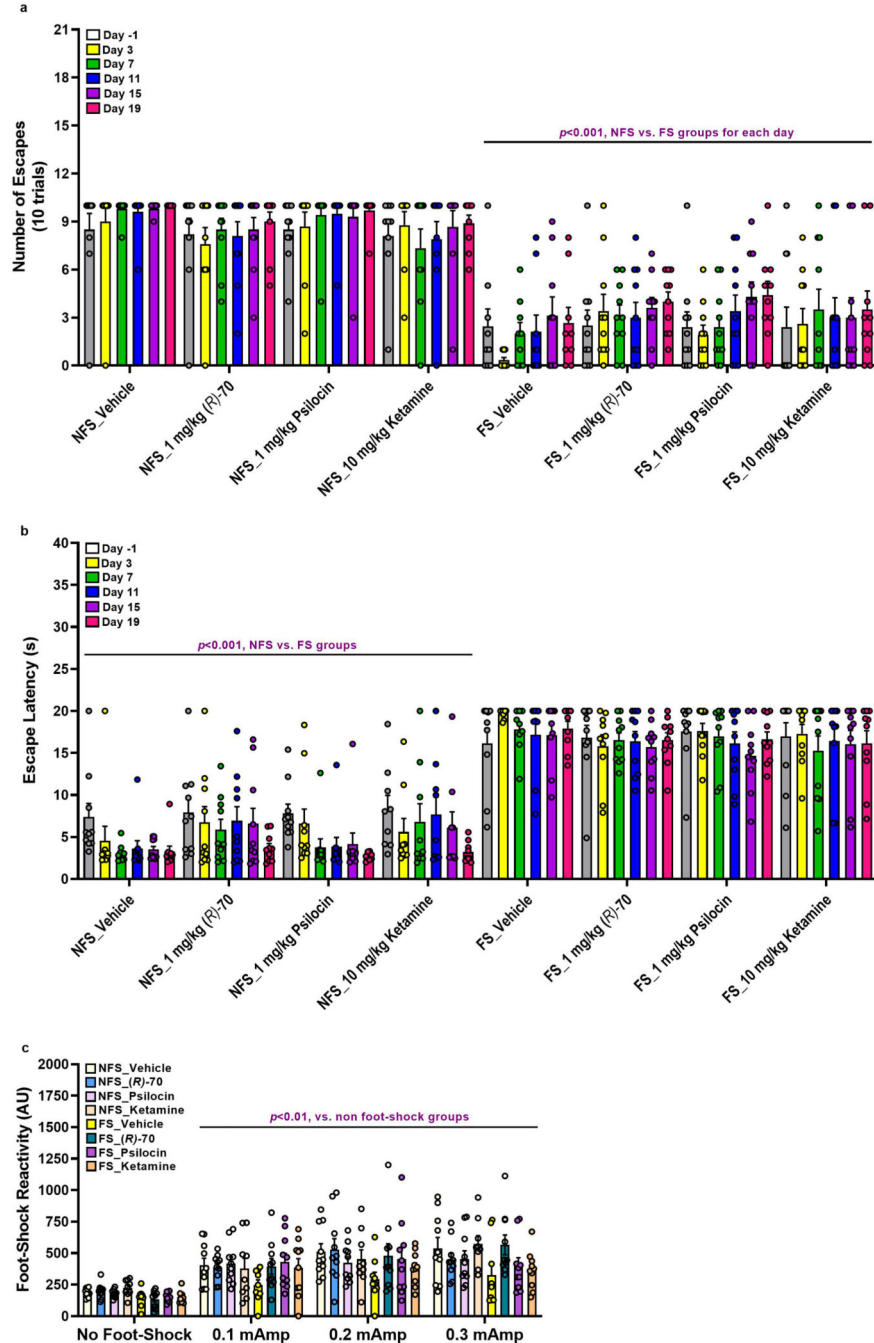
inhibitory effects on locomotion. The compounds blocked LSD-stimulated hyperlocomotion. **(C)** CPP in C57BL/6J mice to 3 mg/Kg **(R)-69**, 3 mg/Kg **(R)-70**, or 20 mg/Kg cocaine (i.p.). No group differences are present at acclimatization, while CPP is evident only in the cocaine group. **(D)** Behavioral sensitization across 5 consecutive days with a challenge on day 11 using C57BL/6J mice treated (i.p.) with 3 mg/Kg **(R)-69** or 20 mg/Kg cocaine. While baseline activities (1 h) are similar between **(R)-69**- and cocaine-treated mice on day 1, baseline locomotion in the latter group is increased across days 2–5 and at challenge on day 11. Locomotor activities (2 h) are low across all post-injection days for **(R)-69** mice, whereby behavioral sensitization to cocaine increases across days 1–3 and remains high through testing. **(R)-69**-injected mice do not show behavioral sensitization. Results presented as mean \pm s.e.m. in the figure, Ns are found in Methods. Primary statistics are in Supplementary Table 4. In the figure the Bonferroni pair-wise corrected p -values (p_s) across multiple comparisons to LSD, LSD + **(R)-69**, or LSD + **(R)-70** showing the value closest to $p < 0.05$ (panel B) or within a single comparison (p) from cocaine on specific days (panels C-D).



Extended Data Figure 9. Anxiety-like behaviors in non-foot-shocked (NFS) and foot-shocked (FS) learned helplessness mice.

(A) Percent time in the open areas in the elevated zero maze with C57BL/6J mice treated (i.p.) with the vehicle, 3 mg/Kg (R)-70, 1 mg/Kg psilocin, or 10 mg/Kg ketamine. Animals are tested 13 days post-injection. Mice in the FS condition spend less time in the open areas than NFS animals. Vehicle-treated FS mice spend less time in the open areas than the (R)-70, psilocin, or ketamine FS animals. (B) Latencies to enter the open areas of the maze. Latencies to enter the open areas are prolonged in the FS mice. (C) Distance traveled in

the maze. FS mice ambulate within the maze over shorter distances than the NSF animals. Results presented as mean \pm s.e.m. in the figure, Ns are provided in the Methods section. Primary statistics are found in Supplementary Table 4. In the figure the Bonferroni pair-wise corrected p -values (p s) across multiple comparisons for vehicle showing the treatment value closest to $p < 0.05$ (panel A) or within a single comparison (p) from condition (panels A-C).



Extended Data Figure 10. Numbers of escapes, latency to escape, and foot-shock reactivity in non-foot-shocked (NFS) and foot-shocked (FS) learned helplessness mice.

(A) Number of escapes from foot-shock in C57BL/6J mice treated (i.p.) with the vehicle, 1 mg/Kg (**R**)-70, 1 mg/Kg psilocin, or 10 mg/Kg ketamine. All mice assigned to the FS condition have fewer escapes from foot-shock than the NFS animals. (B) Latency to escape from foot-shock in the same experiment. All mice in the FS condition have prolonged escape latencies compared to NFS animals. (C) Reactivity to foot-shock in the same experiment. No significant differences in response to foot-shock are detected among treatment groups or between mice in the NFS or FS conditions. All mice exposed to foot-shock (i.e., 0.1–0.3 mAmp) respond at a similar magnitude and this is higher than in the absence of foot-shock (0 mAmp). Results presented as mean \pm s.e.m. in the figure, Ns are provided in the Methods section. Primary statistics are found in Supplementary Table 4. In the figure the Bonferroni pair-wise corrected p -values (p_s) across multiple comparisons to 0 mAmp showing the intensity closest to $p < 0.05$ (panel C) or within a single comparison (p) from condition (panels A-B).

Extended Data Table 1.

Occurrence of THP, piperidine and pyridine containing molecules in different chemical libraries.

Library	Size	No. THPs (%)	No. piperidines (%)	No. pyridines (%)
World drugs*	2953	20 (0.68%)	274 (9.28%)	287 (9.72%)
Natural products [†]	307,815	366 (0.12%)	29,193 (9.48%)	26,049 (8.46%)
In Stock lead-like [‡]	10M	9463 (0.09%)	1.17M (11.7%)	1.28M (12.8%)
Make-on-demand [‡]	1.35B	4.76M (0.35%)	213M (15.8%)	240M (17.8%)

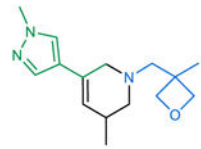
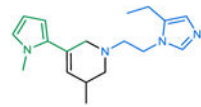
^aFrom <https://zinc20.docking.org/substances/subsets/world>.

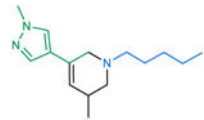
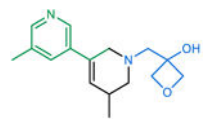
^bFrom <https://zinc20.docking.org/substances/subsets/biogenic>.

^cEnamine REAL, <http://zinc20.docking.org>.

Extended Data Table 2.

Molecules with activity at the 5-HT₂R subtypes identified in the initial screen.

Cmpd	Structure	5-HT _{2A} R		5-HT _{2B} R		5-HT _{2C} R	
		K _i (μ M) pKi \pm S.E.M	EC ₅₀ (μ M) {pEC ₅₀ \pm S.E.M} {E _{max} \pm S.E.M}	K _i (μ M) pKi \pm S.E.M	EC ₅₀ (μ M) {pEC ₅₀ \pm S.E.M} {E _{max} \pm S.E.M}	K _i (μ M) pKi \pm S.E.M	EC ₅₀ (μ M) {pEC ₅₀ \pm S.E.M} {E _{max} \pm S.E.M}
(\pm)-26		ND ^a	ND ^a	3.88 {5.41 \pm 0.09}	1.94 {5.71 \pm 0.12} 48.9% \pm 2.6	ND ^a	ND ^a
(\pm)-27		6.23 {5.21 \pm 0.08}	antagonist	2.67 {5.57 \pm 0.12}	2.98 {5.53 \pm 0.14} 56.3 % \pm 4.1	ND ^a	ND ^a

Cmpd	Structure	5-HT _{2A} R		5-HT _{2B} R		5-HT _{2C} R	
		K _i (μM) pKi ± S.E.M	EC ₅₀ (μM) {pEC ₅₀ ± S.E.M} {E _{max} ± S.E.M}	K _i (μM) pKi ± S.E.M	EC ₅₀ (μM) {pEC ₅₀ ± S.E.M} {E _{max} ± S.E.M}	K _i (μM) pKi ± S.E.M	EC ₅₀ (μM) {pEC ₅₀ ± S.E.M} {E _{max} ± S.E.M}
(±)-28		ND	>10	1.48 {5.83 ± 0.14}	antagonist	ND ^a	ND ^a
(±)-29		ND	ND	0.67 {6.17 ± 0.08}	antagonist	ND ^a	ND ^a

^aND no measurable activity up to 10 μM.

Extended Data Table 3.

Off-target binding profile for compounds (*R*)-69 and (*R*)-70 of 45 receptors tested.

Target	pKi ± SEM	
	(<i>R</i>)-69	(<i>R</i>)-70
5-HT _{1B} R	5.32 ± 0.08	N.D. ^a
5-HT _{1E} R	6.23 ± 0.18	5.90 ± 0.13
5-HT ₆ R	6.46 ± 0.02	5.50 ± 0.11
5-HT _{7A} R	5.84 ± 0.27	5.49 ± 0.14
α _{2A} -adrenergic receptor	5.25 ± 0.12	5.47 ± 0.05
α _{2B} - adrenergic receptor	5.42 ± 0.15	5.71 ± 0.08
α _{2C} - adrenergic receptor	5.73 ± 0.13	5.68 ± 0.14
Histamine H1 receptor	5.89 ± 0.16	6.19 ± 0.01
Histamine H3 receptor	N.D. ^a	5.71 ± 0.02
M3 muscarinic acetylcholine receptor	<5	N.D. ^a
M4 muscarinic acetylcholine receptor	<5	<5
M5 muscarinic acetylcholine receptor	<5	<5
Mu Opioid receptor	5.66 ± 0.07	N.D. ^a
SERT	6.18 ± 0.12	5.69 ± 0.12
Sigma 1 receptor	N.D. ^a	5.53 ± 0.24
Sigma 2 receptor	5.48 ± 0.01	5.89 ± 0.05

45 targets were evaluated for off-target binding by radio-ligand displacement. Those showing better than 50% displacement at 10 μM or lower compound are shown here. The full list of 45 is given in SI Table 5.

^aN.D. no measurable activity up to 10 μM.

Extended Data Table 4.

Cryo-EM data collection, model refinement and validation.

Structure	5HT _{2A} R-miniG _{q/r} -(R)-69
PDB ID	7RAN
Data collection	
Magnification	57,050
Voltage (kV)	300
Dose per frame (e ⁻ /Å ²)	1.20
Electron exposure (e ⁻ /Å ²)	60.01
Defocus Range (µm)	-0.8 to -1.8
Pixel size (Å)	0.8521
Processing software	Relion 3.1
Symmetry imposed	C1
Number of Micrographs	5140
Initial particle images (no.)	4,038,793
Final particle images (no.)	88,393
Map resolution (Å)	3.38 (Mtriage) / 3.45 (Relion)
FSC threshold	0.143
Refinement Statistics [#]	
Model Resolution (Å)	3.5
FSC threshold	0.5
Map sharpening B factor (Å ²)	82.03
Model composition	
Total number of atoms	8523
Protein	8507
Ligand	16
Number of residues	1120
Model validation	
CC (mask) map vs. model (%)	81
R.m.s. deviations	
Bond lengths (Å)	0.003
Bond angles (°)	0.627
Ramachandran plot	
Favored (%)	97
Outlier (%)	0
Rotamer outliers (%)	0
Clash score	4.9
Molprobrity score	1.43

[#]Reported by Phenix comprehensive cryo-EM validation.

Supplementary Material

Refer to Web version on PubMed Central for supplementary material.

Acknowledgements:

Supported by DARPA HR001119S0092 (to BLR, GS, WCW, and BKS) and by NIH grants R35GM122473 (to JAE), R35GM122481 (to BKS), R37DA045657 (to BLR), R01MH11205 (BLR and BKS) and GM71896 (to JJI). Some of the behavioral experiments were conducted with equipment and software purchased with a North Carolina Biotechnology Center grant. The views, opinions, and/or findings contained in this material are those of the authors and should not be interpreted as representing the official views, policies, or endorsement of the Department of Defense or the U.S. Government. We thank Schrodinger for generous donation of its Maestro and FEP+ packages and programs and OpenEye Scientific for generous donation of Omega and OEChem programs. We thank Elizabeth Montabana at the Stanford-SLAC cryo-EM facility for support with data collection. We thank Mitchell Huffstickler, Crisanta Ritter, and Christopher Means for helping with the behavioral testing and Jiechun Zhou for breeding, genotyping, and maintaining the VMAT2 mice. We wish to thank the NIDA Drug Supply Program for providing us with (+)-LSD-(+)-tartrate and psilocin.

JAE, DNC, OSK, BLR, KK, BKS, ALK, and JJI have filed a patent around the new THP agonists through their universities. BKS is a founder of Epiodyne Inc, and with JJI, BlueDolphin, LLC. BKS, JJI and GS are co-founders of Deep Apple Inc. BLR is a Scientific Founder of Onsero Therapeutics.

References

1. Gloriam DE Bigger is better in virtual drug screens. *Nature* 566, 193–194, doi:10.1038/d41586-019-00145-6 (2019).
2. Lyu J. et al. Ultra-large library docking for discovering new chemotypes. *Nature* 566, 224–229, doi:10.1038/s41586-019-0917-9 (2019). [PubMed: 30728502]
3. Gorgulla C. et al. An open-source drug discovery platform enables ultra-large virtual screens. *Nature* 580, 663–668, doi:10.1038/s41586-020-2117-z (2020). [PubMed: 32152607]
4. Stein RM et al. Virtual discovery of melatonin receptor ligands to modulate circadian rhythms. *Nature* 579, 609–614, doi:10.1038/s41586-020-2027-0 (2020). [PubMed: 32040955]
5. Duttwyler S, Lu C, Rheingold AL, Bergman RG & Ellman JA Highly Diastereoselective Synthesis of Tetrahydropyridines by a C–H Activation–Cyclization–Reduction Cascade. *Journal of the American Chemical Society* 134, 4064–4067, doi:10.1021/ja2119833 (2012). [PubMed: 22356093]
6. Duttwyler S. et al. Proton Donor Acidity Controls Selectivity in Nonaromatic Nitrogen Heterocycle Synthesis. *Science* 339, 678, doi:10.1126/science.1230704 (2013). [PubMed: 23393259]
7. Ischay MA, Takase MK, Bergman RG & Ellman JA Unstabilized Azomethine Ylides for the Stereoselective Synthesis of Substituted Piperidines, Tropanes, and Azabicyclo[3.1.0] Systems. *Journal of the American Chemical Society* 135, 2478–2481, doi:10.1021/ja312311k (2013). [PubMed: 23398467]
8. Lovering F, Bikker J. & Humblet C. Escape from Flatland: Increasing Saturation as an Approach to Improving Clinical Success. *Journal of Medicinal Chemistry* 52, 6752–6756, doi:10.1021/jm901241e (2009). [PubMed: 19827778]
9. The structure, bioactivity, literature, and clinical trials of LSD, ergotamine, vinblastine, vincristine, and dehydroemetine can be obtained by searching the compound name in PubChem.
10. Boström J, Brown DG, Young RJ & Keserü GM Expanding the medicinal chemistry synthetic toolbox. *Nature Reviews Drug Discovery* 17, 709–727, doi:10.1038/nrd.2018.116 (2018). [PubMed: 30140018]
11. Sterling T. & Irwin JJ ZINC 15--Ligand Discovery for Everyone. *J Chem Inf Model* 55, 2324–2337, doi:10.1021/acs.jcim.5b00559 (2015). [PubMed: 26479676]
12. Oprea TI, Davis AM, Teague SJ & Leeson PD Is there a difference between leads and drugs? A historical perspective. *J Chem Inf Comput Sci* 41, 1308–1315, doi:10.1021/ci010366a (2001). [PubMed: 11604031]
13. Berger M, Gray JA & Roth BL The expanded biology of serotonin. (2009).
14. McCorvy JD & Roth BL Structure and function of serotonin G protein-coupled receptors. (2015).

15. Meltzer HY & Roth BL Lorcasein and pimavanserin: emerging selectivity of serotonin receptor subtype-targeted drugs. (2013).
16. Kim K.et al. Structure of a Hallucinogen-Activated Gq-Coupled 5-HT_{2A} Serotonin Receptor. *Cell* 182, 1574–1588.e1519, doi:10.1016/j.cell.2020.08.024 (2020). [PubMed: 32946782]
17. Carhart-Harris R.et al. Trial of Psilocybin versus Escitalopram for Depression. (2021).
18. Roth BL Drugs and valvular heart disease. (2007).
19. Rothman RB et al. Evidence for possible involvement of 5-HT(2B) receptors in the cardiac valvulopathy associated with fenfluramine and other serotonergic medications. (2000).
20. Wacker D.et al. Structural features for functional selectivity at serotonin receptors. *Science* 340, 615–619, doi:10.1126/science.1232808 (2013). [PubMed: 23519215]
21. Wacker D.et al. Crystal Structure of an LSD-Bound Human Serotonin Receptor. *Cell* 168, 377–389 e312, doi:10.1016/j.cell.2016.12.033 (2017). [PubMed: 28129538]
22. Andrade R.et al. Vol. 2019(4) (IUPHAR/BPS Guide to Pharmacology, 2019).
23. Mysinger MM, Carchia M, Irwin JJ & Shoichet BK Directory of useful decoys, enhanced (DUD-E): better ligands and decoys for better benchmarking. *J Med Chem* 55, 6582–6594, doi:10.1021/jm300687e (2012). [PubMed: 22716043]
24. Huang XP et al. Allosteric ligands for the pharmacologically dark receptors GPR68 and GPR65. *Nature* 527, 477–483, doi:10.1038/nature15699 (2015). [PubMed: 26550826]
25. Lansu K.et al. In silico design of novel probes for the atypical opioid receptor MRGPRX2. *Nat Chem Biol* 13, 529–536, doi:10.1038/nchembio.2334 (2017). [PubMed: 28288109]
26. Irwin JJ & Shoichet BK Docking Screens for Novel Ligands Conferring New Biology. *J Med Chem* 59, 4103–4120, doi:10.1021/acs.jmedchem.5b02008 (2016). [PubMed: 26913380]
27. Bento AP et al. The ChEMBL bioactivity database: an update. *Nucleic Acids Res* 42, D1083–1090, doi:10.1093/nar/gkt1031 (2014). [PubMed: 24214965]
28. Xu P.et al. Structural insights into the lipid and ligand regulation of serotonin receptors. *Nature* 592, 469–473, doi:10.1038/s41586-021-03376-8 (2021). [PubMed: 33762731]
29. Lassalas P.et al. Evaluation of Oxetan-3-ol, Thietan-3-ol, and Derivatives Thereof as Bioisosteres of the Carboxylic Acid Functional Group. *ACS Medicinal Chemistry Letters* 8, 864–868, doi:10.1021/acsmchemlett.7b00212 (2017). [PubMed: 28835803]
30. Kroeze WK et al. PRESTO-Tango as an open-source resource for interrogation of the druggable human GPCRome. *Nature Structural & Molecular Biology* 22, 362–369, doi:10.1038/nsmb.3014 (2015).
31. Ray TS Psychedelics and the Human Receptorome. *PLOS ONE* 5, e9019, doi:10.1371/journal.pone.0009019 (2010). [PubMed: 20126400]
32. Rodriguiz RM et al. LSD-stimulated behaviors in mice require beta-arrestin 2 but not beta-arrestin 1. *Sci Rep* 11, 17690, doi:10.1038/s41598-021-96736-3 (2021). [PubMed: 34480046]
33. Abel R, Wang L, Harder ED, Berne BJ & Friesner RA Advancing Drug Discovery through Enhanced Free Energy Calculations. *Accounts of Chemical Research* 50, 1625–1632, doi:10.1021/acs.accounts.7b00083 (2017). [PubMed: 28677954]
34. Ballesteros JA & Weinstein H.in *Methods in Neurosciences Vol. 25* (ed Sealfon Stuart C.) 366–428 (Academic Press, 1995).
35. Maeda S.et al. Development of an antibody fragment that stabilizes GPCR/G-protein complexes. *Nature Communications* 9, 3712, doi:10.1038/s41467-018-06002-w (2018).
36. Robertson MJ, van Zundert GCP, Borrelli K.& Skiniotis G.GemSpot: A Pipeline for Robust Modeling of Ligands into Cryo-EM Maps. *Structure* 28, 707–716.e703, doi:10.1016/j.str.2020.04.018 (2020). [PubMed: 32413291]
37. Cao D.et al. Structure-based discovery of nonhallucinogenic psychedelic analogs. *Science* 375, 403–411, doi:10.1126/science.abl8615 (2022). [PubMed: 35084960]
38. Meltzer HY The role of serotonin in antipsychotic drug action. (1999).
39. Nutt D, Erritzoe D.& Carhart-Harris R.Psychedelic Psychiatry’s Brave New World. (2020).
40. Corne SJ & Pickering RW A possible correlation between drug-induced hallucinations in man and a behavioural response in mice. (1967).

41. Woolley DW Production of Abnormal (Psychotic?) Behavior in Mice with Lysergic Acid Diethylamide, and Its Partial Prevention with Cholinergic Drugs and Serotonin. *Proc Natl Acad Sci U S A* 41, 338–344, doi:10.1073/pnas.41.6.338 (1955). [PubMed: 16589676]
42. Roth BL, Willins DL, Kristiansen K.& Kroeze WK Activation is Hallucinogenic and Antagonism is Therapeutic: Role of 5-HT_{2A} Receptors in Atypical Antipsychotic Drug Actions. *The Neuroscientist* 5, 254–262, doi:10.1177/107385849900500414 (1999).
43. Gasser P, Kirchner K.& Passie T.LSD-assisted psychotherapy for anxiety associated with a life-threatening disease: a qualitative study of acute and sustained subjective effects. *J Psychopharmacol* 29, 57–68, doi:10.1177/0269881114555249 (2015). [PubMed: 25389218]
44. Goldberg SB, Pace BT, Nicholas CR, Raison CL & Hutson PR The experimental effects of psilocybin on symptoms of anxiety and depression: A meta-analysis. *Psychiatry Res* 284, 112749, doi:10.1016/j.psychres.2020.112749 (2020).
45. Grob CS et al. Pilot study of psilocybin treatment for anxiety in patients with advanced-stage cancer. *Arch Gen Psychiatry* 68, 71–78, doi:10.1001/archgenpsychiatry.2010.116 (2011). [PubMed: 20819978]
46. Ross S.et al. Rapid and sustained symptom reduction following psilocybin treatment for anxiety and depression in patients with life-threatening cancer: a randomized controlled trial. *J Psychopharmacol* 30, 1165–1180, doi:10.1177/0269881116675512 (2016). [PubMed: 27909164]
47. Shao LX et al. Psilocybin induces rapid and persistent growth of dendritic spines in frontal cortex in vivo. *Neuron*. doi:10.1016/j.neuron.2021.06.008 (2021).
48. Jorgensen WL Efficient drug lead discovery and optimization. *Acc Chem Res* 42, 724–733, doi:10.1021/ar800236t (2009). [PubMed: 19317443]
49. Cutrona KJ, Newton AS, Krimmer SG, Tirado-Rives J.& Jorgensen WL Metadynamics as a Postprocessing Method for Virtual Screening with Application to the Pseudokinase Domain of JAK2. *J Chem Inf Model* 60, 4403–4415, doi:10.1021/acs.jcim.0c00276 (2020). [PubMed: 32383599]
50. Saper NI et al. Nickel-catalysed anti-Markovnikov hydroarylation of unactivated alkenes with unactivated arenes facilitated by non-covalent interactions. *Nat Chem* 12, 276–283, doi:10.1038/s41557-019-0409-4 (2020). [PubMed: 32042137]
51. Yempala T.et al. Dibenzofuranylethylamines as 5-HT_{2A/2C} Receptor Agonists. *ACS Omega* 5, 2260–2266, doi:10.1021/acsomega.9b03430 (2020). [PubMed: 32064387]

References - Methods

52. Sterling T.& Irwin JJ ZINC 15--Ligand Discovery for Everyone. *J Chem Inf Model* 55, 2324–2337, doi:10.1021/acs.jcim.5b00559 (2015). [PubMed: 26479676]
53. Wacker D.et al. Crystal Structure of an LSD-Bound Human Serotonin Receptor. *Cell* 168, 377–389 e312, doi:10.1016/j.cell.2016.12.033 (2017). [PubMed: 28129538]
54. Pei J.& Grishin NV PROMALS3D: multiple protein sequence alignment enhanced with evolutionary and three-dimensional structural information. *Methods Mol Biol* 1079, 263–271, doi:10.1007/978-1-62703-646-7_17 (2014).
55. Wacker D.et al. Structural features for functional selectivity at serotonin receptors. *Science* 340, 615–619, doi:10.1126/science.1232808 (2013). [PubMed: 23519215]
56. Liu W.et al. Serial femtosecond crystallography of G protein-coupled receptors. *Science* 342, 1521–1524, doi:10.1126/science.1244142 (2013). [PubMed: 24357322]
57. Webb B.& Sali A.Comparative Protein Structure Modeling Using MODELLER. *Current protocols in bioinformatics / editorial board, Andreas D. Baxevanis ... [et al.]* 47, 5 6 1–5 6 32, doi:10.1002/0471250953.bi0506s47 (2014).
58. Coleman RG, Carchia M, Sterling T, Irwin JJ & Shoichet BK Ligand pose and orientational sampling in molecular docking. *PLoS One* 8, e75992, doi:10.1371/journal.pone.0075992 (2013).
59. Southan C.et al. The IUPHAR/BPS Guide to PHARMACOLOGY in 2016: towards curated quantitative interactions between 1300 protein targets and 6000 ligands. *Nucleic Acids Res* 44, D1054–1068, doi:10.1093/nar/gkv1037 (2016). [PubMed: 26464438]

60. Mysinger MM, Carchia M, Irwin JJ & Shoichet BK Directory of useful decoys, enhanced (DUD-E): better ligands and decoys for better benchmarking. *J Med Chem* 55, 6582–6594, doi:10.1021/jm300687e (2012). [PubMed: 22716043]
61. Case DA et al. AMBER 2015. (2015).
62. Mysinger MM & Shoichet BK Rapid context-dependent ligand desolvation in molecular docking. *J Chem Inf Model* 50, 1561–1573, doi:10.1021/ci100214a (2010). [PubMed: 20735049]
63. Wei BQ, Baase WA, Weaver LH, Matthews BW & Shoichet BK A model binding site for testing scoring functions in molecular docking. *J Mol Biol* 322, 339–355, doi:10.1016/s0022-2836(02)00777-5 (2002). [PubMed: 12217695]
64. Word JM, Lovell SC, Richardson JS & Richardson DC Asparagine and glutamine: using hydrogen atom contacts in the choice of side-chain amide orientation1. *Journal of Molecular Biology* 285, 1735–1747, doi:10.1006/jmbi.1998.2401 (1999). [PubMed: 9917408]
65. Gallagher K. & Sharp K. Electrostatic contributions to heat capacity changes of DNA-ligand binding. *Biophys J* 75, 769–776, doi:10.1016/S0006-3495(98)77566-6 (1998). [PubMed: 9675178]
66. Sharp KA Polyelectrolyte electrostatics: Salt dependence, entropic, and enthalpic contributions to free energy in the nonlinear Poisson–Boltzmann model. *Biopolymers* 36, 227–243, doi:10.1002/bip.360360210 (1995).
67. Pettersen EF et al. UCSF Chimera—A visualization system for exploratory research and analysis. *Journal of Computational Chemistry* 25, 1605–1612, doi:10.1002/jcc.20084 (2004). [PubMed: 15264254]
68. Bento AP et al. The ChEMBL bioactivity database: an update. *Nucleic Acids Res* 42, D1083–1090, doi:10.1093/nar/gkt1031 (2014). [PubMed: 24214965]
69. Olsson MHM, Søndergaard CR, Rostkowski M. & Jensen JH PROPKA3: Consistent Treatment of Internal and Surface Residues in Empirical PKa Predictions. *Journal of Chemical Theory and Computation* 7, 525–537 (2011). [PubMed: 26596171]
70. Abel R, Wang L, Harder ED, Berne BJ & Friesner RA Advancing Drug Discovery through Enhanced Free Energy Calculations. *Accounts of Chemical Research* 50, 1625–1632, doi:10.1021/acs.accounts.7b00083 (2017). [PubMed: 28677954]
71. Wang L. et al. Accurate and Reliable Prediction of Relative Ligand Binding Potency in Prospective Drug Discovery by Way of a Modern Free-Energy Calculation Protocol and Force Field. *J Am Chem Soc* 137, 2695–2703 (2015). [PubMed: 25625324]
72. Duttwyler S, Lu C, Rheingold AL, Bergman RG & Ellman JA Highly Diastereoselective Synthesis of Tetrahydropyridines by a C–H Activation–Cyclization–Reduction Cascade. *Journal of the American Chemical Society* 134, 4064–4067, doi:10.1021/ja2119833 (2012). [PubMed: 22356093]
73. Duttwyler S. et al. Proton Donor Acidity Controls Selectivity in Nonaromatic Nitrogen Heterocycle Synthesis. *Science* 339, 678, doi:10.1126/science.1230704 (2013). [PubMed: 23393259]
74. Ischay MA, Takase MK, Bergman RG & Ellman JA Unstabilized Azomethine Ylides for the Stereoselective Synthesis of Substituted Piperidines, Tropanes, and Azabicyclo[3.1.0] Systems. *Journal of the American Chemical Society* 135, 2478–2481, doi:10.1021/ja312311k (2013). [PubMed: 23398467]
75. Olsen RHJ et al. TRUPATH, an open-source biosensor platform for interrogating the GPCR transducerome. *Nature Chemical Biology* 16, 841–849, doi:10.1038/s41589-020-0535-8 (2020). [PubMed: 32367019]
76. Zhang Y, Yang Z, Gao X. & Wu G. The role of 5-hydroxytryptamine1A and 5-hydroxytryptamine1B receptors in modulating spinal nociceptive transmission in normal and carrageenan-injected rats. *Pain* 92, 201–211, doi:10.1016/s0304-3959(01)00259-7 (2001). [PubMed: 11323141]
77. Maeda S. et al. Development of an antibody fragment that stabilizes GPCR/G-protein complexes. *Nature Communications* 9, 3712, doi:10.1038/s41467-018-06002-w (2018).
78. Mastrorarde DN Automated electron microscope tomography using robust prediction of specimen movements. *J Struct Biol* 152, 36–51 (2005). [PubMed: 16182563]

79. Zivanov J. et al. New tools for automated high-resolution cryo-EM structure determination in RELION-3. *eLife* 7, e42166, doi:10.7554/eLife.42166 (2018).
80. Zheng SQ et al. MotionCor2: anisotropic correction of beam-induced motion for improved cryo-electron microscopy. *Nature Methods* 14, 331–332, doi:10.1038/nmeth.4193 (2017). [PubMed: 28250466]
81. Kim K. et al. Structure of a Hallucinogen-Activated Gq-Coupled 5-HT_{2A} Serotonin Receptor. *Cell* 182, 1574–1588.e1519, doi:10.1016/j.cell.2020.08.024 (2020). [PubMed: 32946782]
82. Emsley P, Lohkamp B, Scott WG & Cowtan K. Features and development of Coot. *Acta Crystallographica Section D* 66, 486–501, doi:10.1107/S0907444910007493 (2010).
83. Liebschner D. et al. Macromolecular structure determination using X-rays, neutrons and electrons: recent developments in Phenix. *Acta Crystallographica Section D* 75, 861–877, doi:10.1107/S2059798319011471 (2019).
84. Williams CJ et al. MolProbity: More and better reference data for improved all-atom structure validation. *Protein Science* 27, 293–315, doi:10.1002/pro.3330 (2018). [PubMed: 29067766]
85. Pettersen EF et al. UCSF ChimeraX: Structure visualization for researchers, educators, and developers. *Protein Science* 30, 70–82, doi:10.1002/pro.3943 (2021). [PubMed: 32881101]
86. Robertson MJ, van Zundert GCP, Borrelli K. & Skiniotis G. GemSpot: A Pipeline for Robust Modeling of Ligands into Cryo-EM Maps. *Structure* 28, 707–716.e703, doi:10.1016/j.str.2020.04.018 (2020). [PubMed: 32413291]
87. Fukui M. et al. Vmat2 heterozygous mutant mice display a depressive-like phenotype. *J Neurosci* 27, 10520–10529, doi:10.1523/JNEUROSCI.4388-06.2007 (2007). [PubMed: 17898223]
88. Rodriguiz RM et al. LSD-stimulated behaviors in mice require beta-arrestin 2 but not beta-arrestin 1. *Sci Rep* 11, 17690, doi:10.1038/s41598-021-96736-3 (2021). [PubMed: 34480046]
89. Berezniuk I. et al. ProSAAS-derived peptides are regulated by cocaine and are required for sensitization to the locomotor effects of cocaine. *J Neurochem* 143, 268–281, doi:10.1111/jnc.14209 (2017). [PubMed: 28881029]
90. Pogorelov VM et al. 5-HT_{2C} Agonists Modulate Schizophrenia-Like Behaviors in Mice. *Neuropsychopharmacology* 42, 2163–2177, doi:10.1038/npp.2017.52 (2017). [PubMed: 28294132]
91. Wetsel WC et al. Disruption of the expression of the proprotein convertase PC7 reduces BDNF production and affects learning and memory in mice. *Proc Natl Acad Sci U S A* 110, 17362–17367, doi:10.1073/pnas.1314698110 (2013). [PubMed: 24101515]

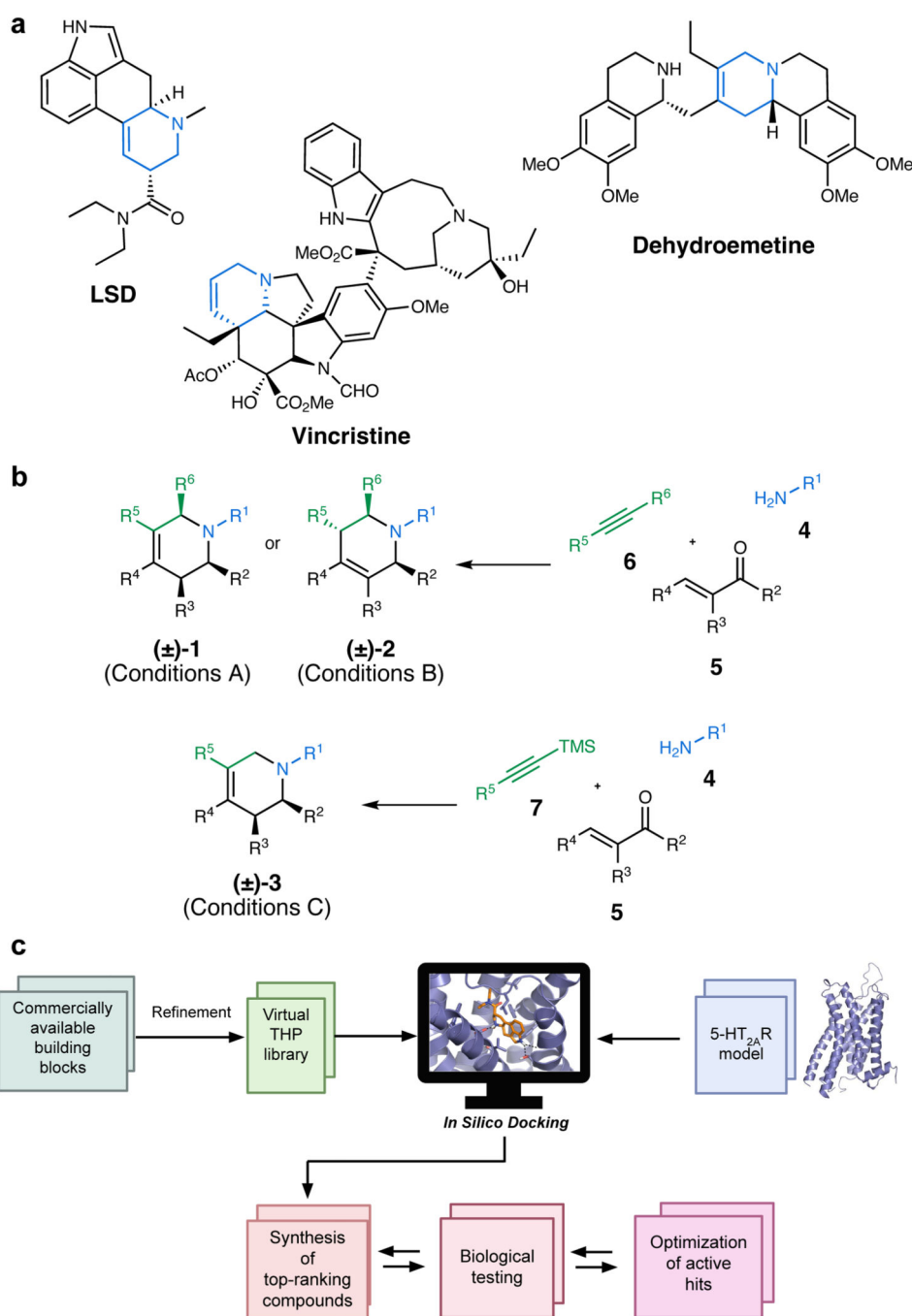


Figure 1. Bespoke ultra-large virtual library approach.

(A) Drugs containing a tetrahydropyridine motif. (B) Three types of tetrahydropyridines (±)-1 to (±)-3 from commercially available alkynes **6** and **7**, primary amines **4**, and α,β -unsaturated carbonyl compounds **5**. (C) Generation of a virtual library of 75 million tetrahydropyridines for docking against a homology model of the 5-HT_{2A}R.

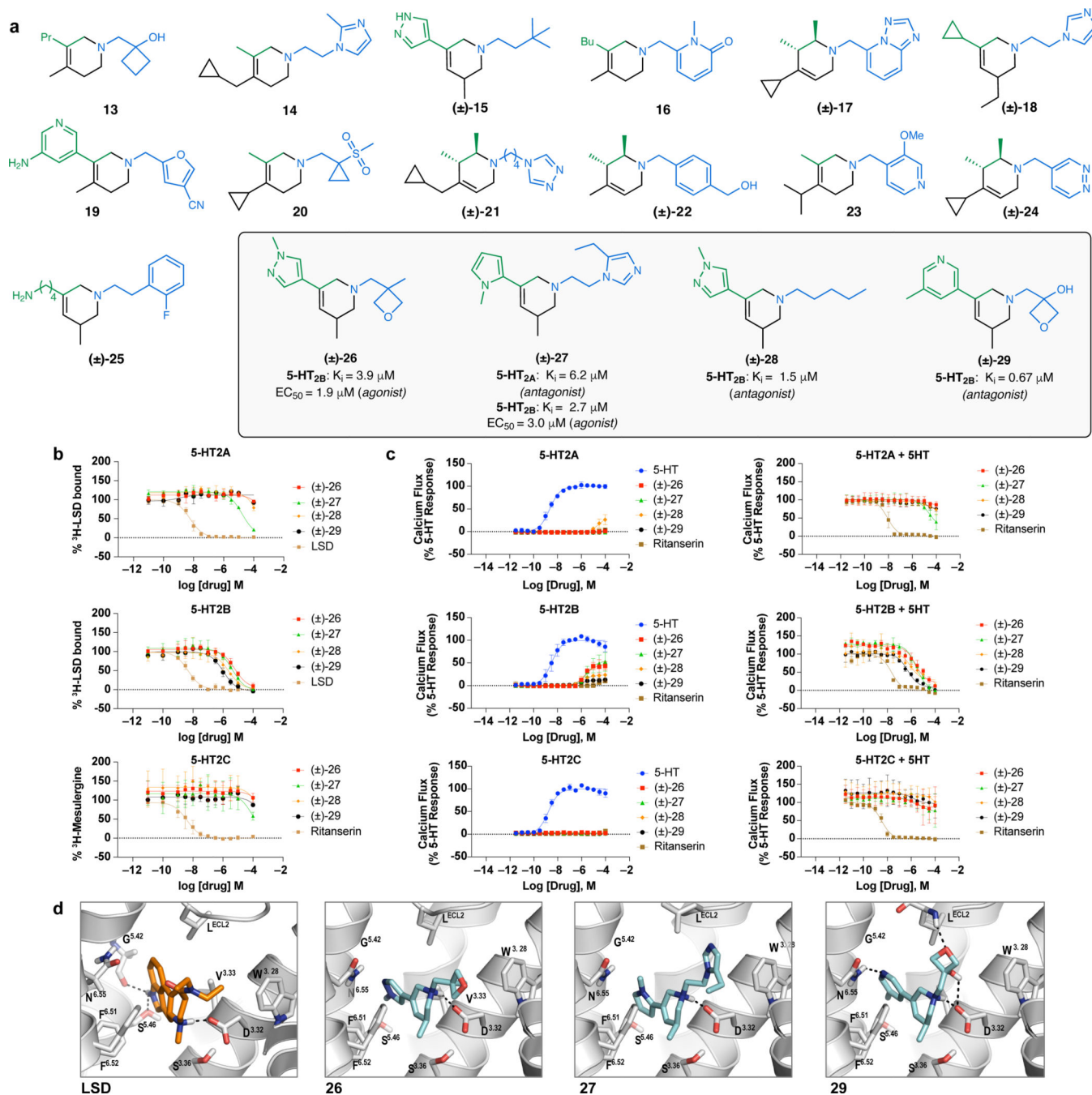


Figure 2. Large scale docking screen of a THP virtual library discovers new 5-HT_{2R} ligands. (A) The initial 17 compounds synthesized and assayed; of these four had 5-HT_{2A}R or 5-HT_{2B}R activity (boxed). (B) Binding of the four actives at human 5-HT_{2R}s in radioligand competition binding assays. Concentration-inhibition curves at 5-HT_{2A}R and 5-HT_{2B}R versus [³H]-LSD, and 5-HT_{2C}R versus [³H]- Mesulergine. [³H]-LSD, and [³H]-Mesulergine concentrations of 0.5 nM, and 1.0 nM were used, respectively. K_D values of [³H]-LSD at human 5-HT_{2A}R and 5-HT_{2B}R were 0.33 and 0.91 nM, respectively, and K_D value of [³H]-mesulergine at human 5-HT_{2C}R was 0.67 nM^{21,51}. LSD (5-HT_{2A}R, 5-HT_{2B}R)

and Ritanserin (5-HT_{2C}R) were used as positive controls. **(C)** Concentration-response curves of the four actives at stable 5-HT_{2A}R, 5-HT_{2B}R, and 5-HT_{2C}R-INI Flp-In293 cell lines in Ca²⁺ assays. Data in **(B)** and **(C)** represent the mean \pm S.E.M from n=3 independent experiments. **(D)** Docked poses of characteristic molecules compared to that of LSD (left panel). In all panels, Ballesteros-Weinstein residue numbering is shown in superscript.

Author Manuscript

Author Manuscript

Author Manuscript

Author Manuscript

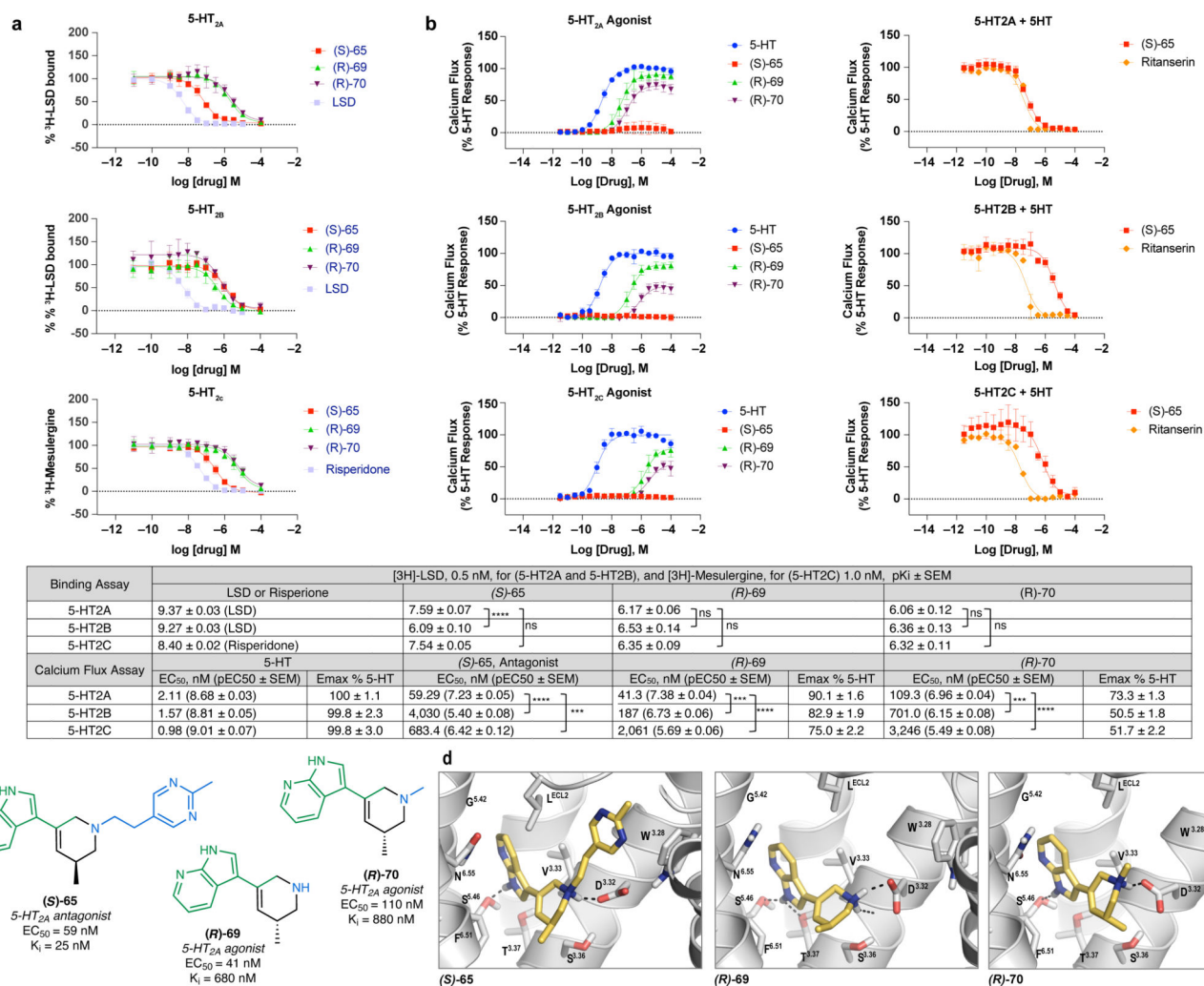


Figure 3. Structure-guided discovery of 5-HT_{2A}R agonists and antagonists.

(A) Dose response competition binding assays of (S)-65, (R)-69, and (R)-70 against [³H]-LSD for 5-HT_{2A}R and 5-HT_{2B}R, and [³H]-Mesulergine for 5-HT_{2C}R. [³H]-LSD and [³H]-Mesulergine concentrations of 0.3 nM and 1 nM were used, respectively. LSD (5-HT_{2A}R, 5-HT_{2B}R) and Risperidone (5-HT_{2C}R) were used as positive controls. (B) Concentration-response curves of (S)-65, (R)-69, and (R)-70 at stable 5-HT_{2A}R, 5-HT_{2B}R, and 5-HT_{2C}R-INI Flp-In293 cell lines in Ca²⁺ assays. (R)-69 and (R)-70 are strong partial G_q agonists, whereas (S)-65 acts as an antagonist. Data in (A) and (B) represent the mean ± S.E.M. from n=3 independent experiments. The pKi/EC₅₀ values between 5-HT_{2A}R, 5-HT_{2B}R and 5-HT_{2C}R were compared using a one-way ANOVA with Dunnett's post-test (* = p<0.05, ** = p<0.01, *** = p<0.001, and **** = p<0.0001). (C) 2D structures, binding and functional affinities for the new ligands across the 5-HT₂R subtypes. (D) Docking poses of (S)-65 (left panel), (S)-69 (the better scoring enantiomer; middle panel) and (R)-70 (right panel). 5-HT_{2A}R is shown in gray, the docked compounds are shown as capped sticks with carbons in yellow. In all panels the Ballesteros-Weinstein residue numbering is shown in superscript.

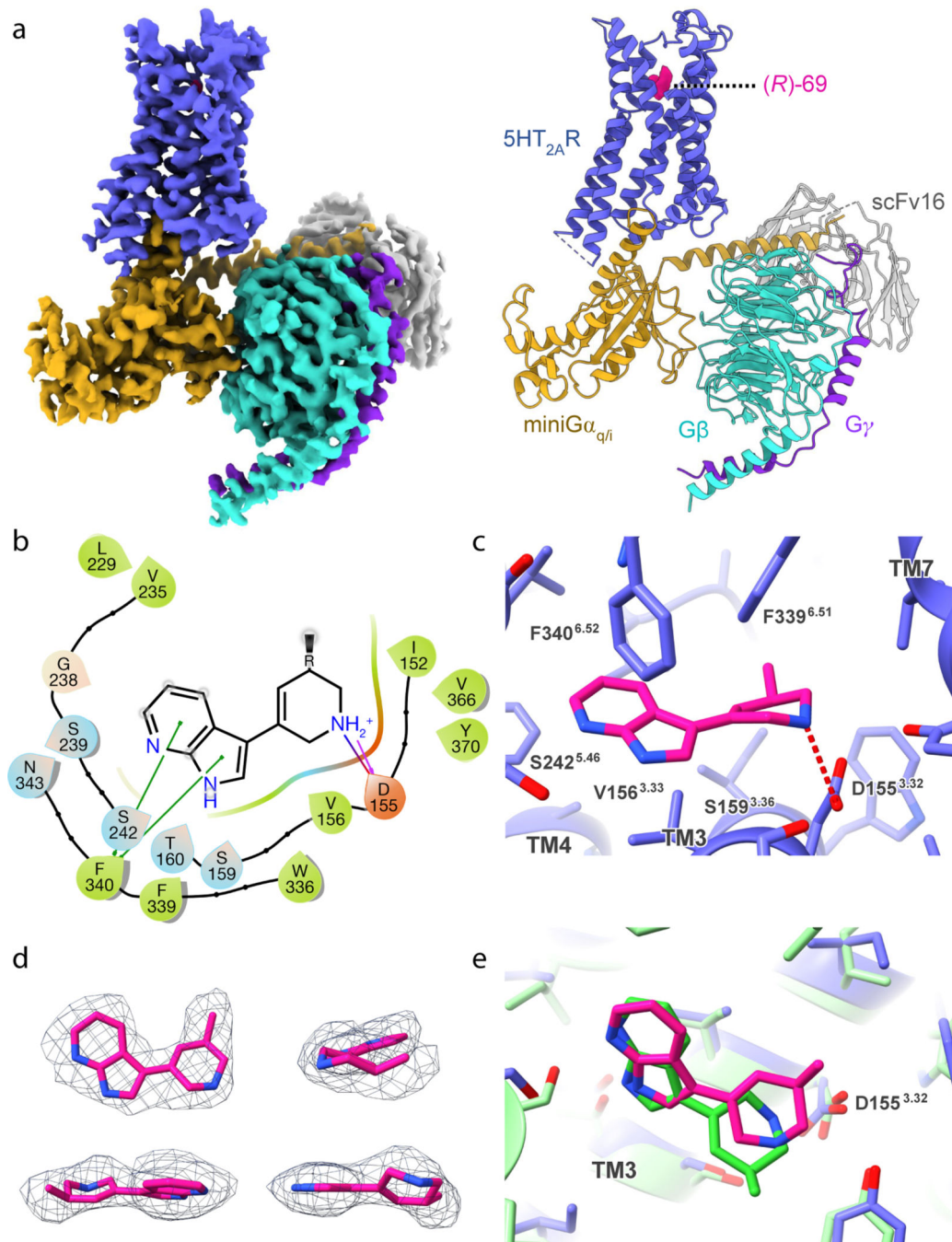


Figure 4. Structure of 5-HT_{2A}R bound to (R)-69 by cryo-EM.

(A) Overall cryo-EM map (left) and model (right) of 5-HT_{2A}R bound to (R)-69 in complex with mini-G_{q/i}. (B) Schematic of ligand-specific interactions of (R)-69 with 5-HT_{2A}R orthosteric residues. A salt bridge with D155^{3.32} is shown as a red dashed line. Color code for residues and interactions: green: hydrophobic, blue: polar, red: negatively charged, grey: glycine, green solid line: Pi-Pi stacking interaction. (C) Specific residues in the binding pocket that interact with (R)-69 are shown as sticks and labeled. (R)-69 is shown as magenta-colored sticks. A salt bridge with D155^{3.32} is shown as a red dashed line.

(D) Cryo-EM density for **(R)-69**. **(E)** Comparison of the computationally predicted and experimentally resolved binding poses of **(S)-69** and **(R)-69**, respectively. The cryo-EM structure in magenta is superposed on **(S)-69** docked to the 5-HT_{2A}R homology model in green. Ballesteros-Weinstein residue numbering is in superscript in panels **(C)** and **(E)**.

Author Manuscript

Author Manuscript

Author Manuscript

Author Manuscript

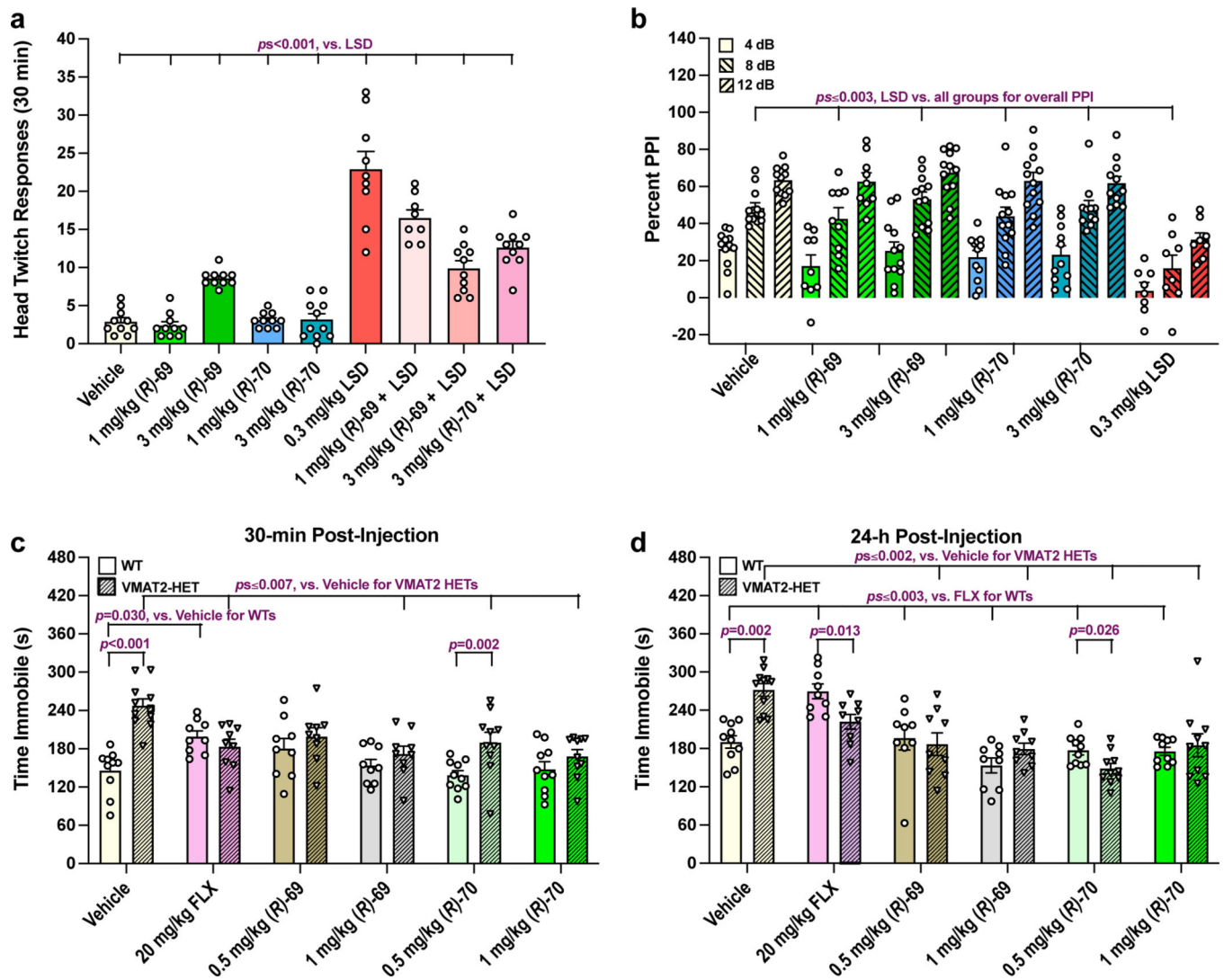


Figure 5. Head twitch, PPI responses, and anti-depressant-like actions of (R)-69 and (R)-70 in mice.

(A) Head twitch responses (HTRs) in C57BL/6J mice during the first 30 min after injection (i.p.) of vehicle, 1 or 3 mg/Kg (R)-69, 1 or 3 mg/Kg (R)-70, 0.3 mg/Kg LSD, 1 or 3 mg/Kg (R)-69 + 0.3 mg/Kg LSD, or 3 mg/Kg (R)-70 + 0.3 mg/Kg LSD. HTRs are low in (R)-69 and (R)-70 groups and they partially block the LSD effects. (B) PPI in C57BL/6J mice treated (i.p.) with vehicle, 1 or 3 mg/Kg (R)-69, 1 or 3 mg/Kg (R)-70, or LSD. PPI is unaffected with (R)-69 or (R)-70 relative to vehicle and LSD disruption. (C-D) Immobility in tail suspension at 30 min and 24 h with WT and VMAT2 heterozygous (HET) mice after a single injection (i.p.) of vehicle, 20 mg/Kg fluoxetine (FLX), 0.5 or 1 mg/Kg (R)-69, or 0.5 or 1 mg/Kg (R)-70. Acute genotype differences are seen with vehicle and 0.5 mg/Kg (R)-70; at 24 h effects are present with vehicle, FLX, and 0.5 mg/Kg (R)-70. In WT mice immobility is enhanced with acute administration of FLX relative to vehicle and at 24 h it is increased with FLX compared to all other groups. In VMAT2 HETs, 30-min after administration FLX, 1 mg/Kg (R)-69, and 0.5 and 1 mg/Kg (R)-70 reduce immobility and at 24 h 0.5 and 1 mg/Kg (R)-69 and (R)-70 are efficacious compared to vehicle. Results presented as mean

\pm s.e.m. in the figure, Ns are provided in Methods section. Primary statistics are found in Supplementary Table 4. In this figure the Bonferroni pair-wise corrected p -values (ps) across multiple comparisons for LSD, vehicle, or FLX are depicted for the value closest to $p < 0.05$ (panels **A-D**) or within a single comparison (p) between or within genotypes (panels **C-D**).

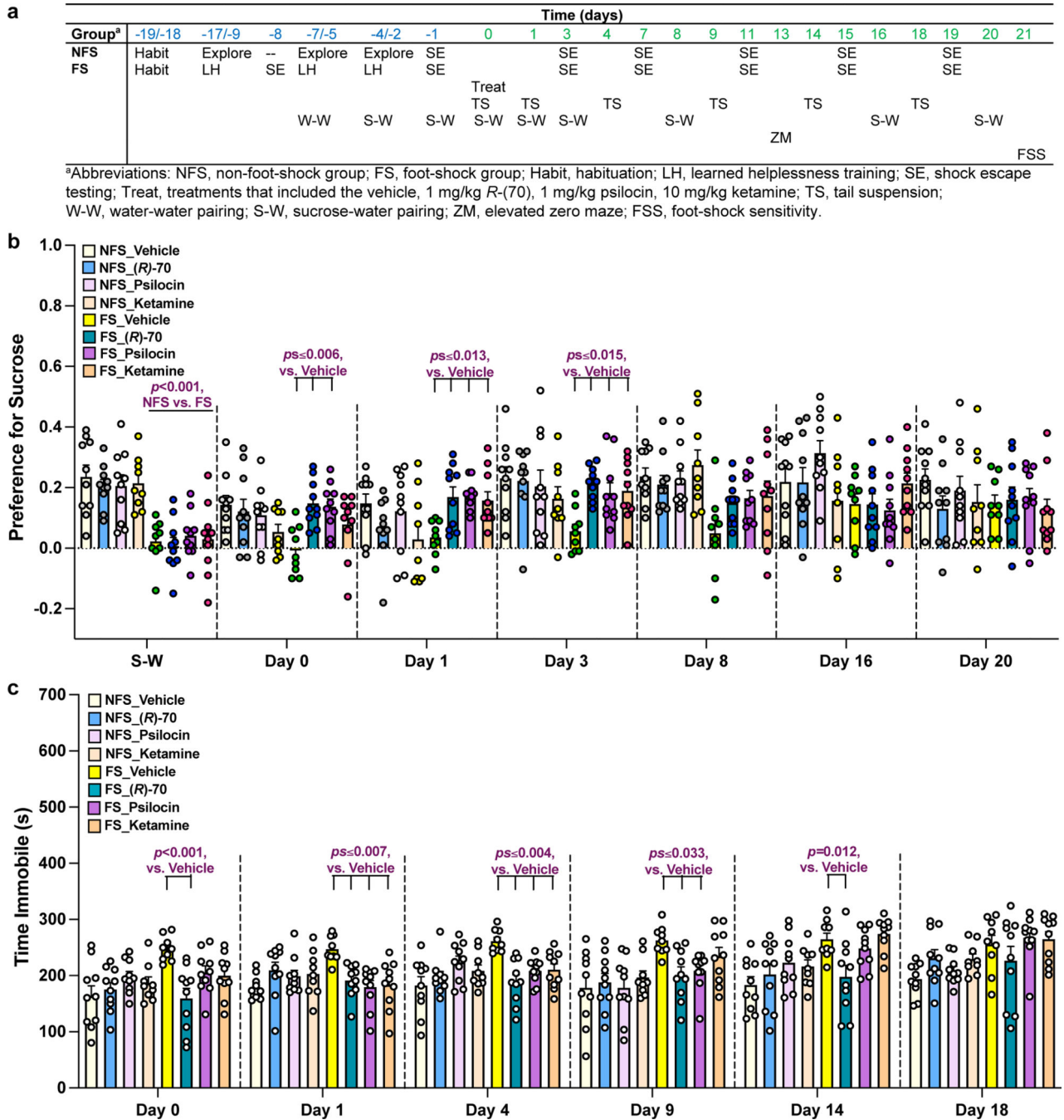


Figure 6. Experimental design, sucrose preference, and tail suspension for the learned helplessness experiment.

(A) Experimental design. (B) Sucrose preference in C57BL/6 mice assigned to the non-foot-shock (NFS) and foot-shock (FS) conditions and treated (i.p.) with vehicle, 1 mg/Kg *R*-70, 1 mg/Kg psilocin, or 10 mg/Kg ketamine. During the initial sucrose-water (S-W) pairing, mice in the FS condition have a lower preference for sucrose than the NFS mice. Among the NFS animals, no treatment effects are found within days. By comparison among FS mice, sucrose preference is reduced in the vehicle controls compared to the *R*-70 and psilocin

groups on days 0, 1, and 3. The effects of ketamine are delayed but become manifest on days 1 and 3. (C) Tail suspension testing in the same mice. Times of immobility are low and stable across time in the NFS mice. In the FS condition, 30-min following treatment (day 0), immobility is high in the vehicle control relative to the (R)-70 group and this effect persists through day 14. Relative to the FS vehicle control, psilocin and ketamine show efficacy on days 1 and 4, with the effects of psilocin lasting to day 9 post-injection. Results presented as mean \pm s.e.m. in the figure, Ns are provided in the Methods section. Primary statistics are found in Supplementary Table 4. In the figure the Bonferroni pair-wise corrected p -values (p_s) across multiple comparisons to vehicle showing the value closest to $p < 0.05$ within the FS condition or within a single comparison (p) from the vehicle (panels B-C) or condition (panel B).